remote sensing

MDPI

Article

BDS-3 Time Group Delay and Its Effect on Standard Point Positioning

Peipei Dai [1,2,3], Yulong Ge [1,2,3,*], Weijin Qin [1] and Xuhai Yang [1,4]

1 National Time Service Center, Chinese Academy of Sciences, Xi'an 710600, China
2 University of Chinese Academy of Sciences, Beijing 100049, China
3 Key Laboratory of Precise Positioning and Timing Technology, Chinese Academy of Sciences, Xi'an 710600, China
4 School of Astronomy and Space Science, University of Chinese Academy of Sciences, Beijing 100049, China
* Correspondence: geyulong15@mails.ucas.ac.cn; Tel.: +89-029-83893326

Received: 4 June 2019; Accepted: 1 August 2019; Published: 3 August 2019

Abstract: The development of the BeiDou navigation system (BDS) is divided into three phases: The demonstration system (BDS-1), the regional system (BDS-2) and the global BeiDou navigation system (BDS-3). At present, the construction of the global BeiDou navigation system (BDS-3) constellation network is progressing very smoothly. The signal design and functionality of BDS-3 are different from those of BDS-1 and BDS-2. The BDS-3 satellite not only broadcasts B1I (1561.098 MHz) and B3I (1268.52 MHz) signals but also broadcasts new signals B1C (1575.42 MHz) and B2a (1176.45 MHz). In this work, six tracking stations of the international GNSS monitoring and assessment system (iGMAS) were selected, and 41 consecutive days of observation data, were collected. To fully exploit the code observations of BDS-2 and BDS-3, the time group delay (TGD) correction model of BDS-2 and BDS-3 are described in detail. To further verify the efficacy of the broadcast TGD parameters in the broadcast ephemeris, the standard point positioning (SPP) of all the signals from BDS-2 and BDS-3 with and without TGD correction was studied. The experiments showed that the B1I SPP accuracy of BDS-2 was increased by approximately 50% in both the horizontal and vertical components, and B1I/B3I were improved by approximately 70% in the horizontal component and 47.4% in the vertical component with TGD correction. The root mean square (RMS) value of B1I and B1C from BDS-3 with TGD correction was enhanced by approximately 60%–70% in the horizontal component and by approximately 50% in the vertical component. The B2a-based SPP was increased by 60.2% and 64.4% in the east and north components, respectively, and the up component was increased by approximately 19.8%. For the B1I/B3I and B1C/B2a dual-frequency positioning accuracy with TGD correction, the improvement in the horizontal component ranges from 62.1% to 75.0%, and the vertical component was improved by approximately 45%. Furthermore, the positioning accuracy of the BDS-2 + BDS-3 combination constellation was obviously higher than that of BDS-2 or BDS-3.

Keywords: BDS-3; BDS-2 + BDS-3; time group delay; standard point positioning

1. Introduction

The BeiDou constellation began providing positioning, navigation and timing (PNT) services at least in the Asia-Pacific region in December 2012 [1]. The development of the BeiDou constellation has three phases: The BeiDou satellite navigation experimental system (BDS-1), the construction of the regional BeiDou system (BDS-2) and the construction of a global BeiDou system (BDS-3) [2]. By the end of 2012, BDS-2 consisted of five geostationary earth orbits (GEOs), five inclined geosynchronous orbits (IGSOs) and four medium altitude earth orbit (MEO) satellites. The BDS-3 constellation started in 2015 and is expected to provide global service with 5 GEO, 3 IGSO and 27 MEO satellites by 2020 [3]. With

the rapid development of the BDS-2 constellation, BDS-2 has become a hot topic in the GNSS application community [4–6]. Many studies on BDS-2 have been carried out. Zhao et al. [7] presented the initial results of the BDS-2 precise orbit determination (POD). With the precise orbit and clock released by the IGS multi-GNSS experiment (MGEX), it provides the conditions for the study of the precise application of BDS-2 [8,9]. In addition, Guo et al. [10] investigated the effectiveness of the broadcast time group delay (TGD) in the navigation message and differential code biases (DCBs) provided by the MGEX; both the standard point positioning (SPP) and precise point positioning (PPP) were carried out for BDS signals with and without code bias correction. In addition, the triple-frequency ambiguity resolution performance using real BDS-2 data was investigated by Zhang et al. [11]. They illustrated that a minor improvement could be achieved by using triple-frequency observations compared with using dual-frequency observations. Furthermore, Manzino et al. [12] concluded that the GPS-BDS PPP combination presented a slightly better performance in comparable conditions and smaller intervals with the static model. Moreover, a special problem for BDS-2 is the satellite-induced code bias, which was investigated by Wanninger and Beer [13].

Before the launch of the BDS-3 satellites, the experimental BDS-3 (BDS-3e) system consisting of 3 MEO and 2 IGSO satellites was launched [14–16]. Since 2015, BDS-3e has implemented and validated new modes of navigation signals and inter-satellite links. In the last few years, many studies on BDS-3e have been carried out [14–16]. Li et al. [3] analysed the POD for the BDS-3e satellites with the international GNSS continuous monitoring and assessment system (iGMAS) and MGEX tracking networks. In addition, Xu et al. [16] presented the performances of the POD and PPP of the onboard BDS-3e satellites. Precise orbit and clock determination for BDS-3e satellites with yaw attitude using the extend center for orbits determination in Europe (CODE) orbit model (ECOM) has been illustrated by Zhao et al. [17]. Interestingly, there is no satellite-induced code bias in the BDS-3e satellites. From multipath-free conditions, the satellite-induced code variations that still exist in the bands of B1C, B2a and B2b of BDS-3e satellites were investigated by Zhou et al. [18]. Furthermore, Yang et al. [2] studied the performances of the BDS-3 demonstration system, including the signal-to-noise ratios, code errors and the multipath errors of the civilian signals. Moreover, the DCBs and the performance of both satellites and the receiver DCBs for BDS-3e using iGMAS and MEGX network observation data were evaluated by Li et al. [19]. The results showed that the DCBs estimated from the BDS-3e satellite were more stable than those from the BDS-2 satellite.

However, the BDS-3e satellite is not part of the BDS-3 constellation. From November 2017 to May 2019, 18 MEO, 1 GEO and 1 IGSO BDS-3 satellites (excluding experimental satellites) have been launched successfully. As a global system, BDS-3 has provided basic services to the countries along the Belt and Road and the neighboring regions since the end of 2018. The basic status information of the BDS-3 satellites is listed in Table 1. A new satellite attitude mode, signals, and atomic clocks have been applied on the BDS-3 satellite. Five frequencies are used to transmit signals: Backward-compatible old signals B1I (1561.098 MHz) and B3I (1268.52 MHz) and three new open service signals B1C (1575.42 MHz), B2a (1176.45 MHz) and B2b (1207.14 MHz). The B3I signal of the BDS-3 satellites is consistent with that of BDS-2, which uses binary phase-shift keying (BPSK) modulation according to the B3I Interface Control Document (ICD) [20]. The B1C signal has two signal components: A data component (B1C_data) and a pilot component (B1C_pilot), which use the binary offset carrier (BOC) and a quadrature multiplexed binary offset carrier (QMBOC) modulation, respectively, according to the B1C ICD [21]. Similar to the B1C signal, the B2a signal also has two signal components, a data component (B2a_data) and a pilot component (B2a_pilot), but the B2a signal components use the same modulation mode BPSK according to the B2a ICD [22]. The B1C signal shares the same frequency as the GPS L1 and Galileo E1 signals; the B2a signal matches the GPS L5 and Galileo E5a signals; and the B2b signal is compatible with the Galileo E5b signal. Similarly, the BDS-3 B2b signal also matches the BDS-2 B2I signal but uses a different modulation type [23]. The frequencies, signal components, modulations, wavelengths and chip rates of the BDS-3 open service signals are listed in Table 2. Xie et al. [23] analysed the characterization of the BDS-3 satellite GNSS signals with the iGMAS network. The results indicated that the satellite-induced

code bias was negligible at all signals of the BDS-3 satellite, while BDS-3 triple-carrier combinations of small inter-frequency clock bias (IFCB) variations with peak amplitudes of approximately 1 cm can be recognized. Ye et al. [24] analysed the orbits of two BDS-3 satellites, C27 and C28, and the results showed that the median of the observed residuals computed using code observations and the solved initial orbits were better than four, when the new code signal was utilized. Until now, BDS-3e has been analysed by many experts and scholars. However, limited research has focused on BDS-3 satellites, especially for the TGD correction. GNSS (e.g., GPS, GLONASS, BDS and Galileo) codes are well known to be affected by TGD parameters. The TGD correction model for GPS, BDS-2 and Galileo was investigated in detail by Guo et al. [10]. Nevertheless, the TGD correction model of the old signals and new signals of BDS-3 have not been summarized and investigated in detail. From this background, the aim of this paper is to investigate the impact of TGD correction on BDS-3 positioning.

Table 1. Satellite status of the global BeiDou system (BDS-3) (as of May 2019).

Satellite	SVN	Int.sat.ID	NORAD.ID	Manuf.	PRN	Notes
MEO-2	C202	2017-069B	43002	CAST	C20	Slot B-8; launched 5 November 2017
MEO-1	C201	2017-069A	43001	CAST	C19	SlotB-7; launched 5 November 2017
MEO-7	C203	2018-003A	43107	SECM	C27	Slot A-4; launched 12 January 2018
MEO-8	C204	2018-003B	43108	SECM	C28	Slot A-5; launched 12 January 2018
MEO-4	C205	2018-018A	43207	CAST	C22	Slot B-6; launched 12 February 2018
MEO-3	C206	2018-018B	43208	CAST	C21	Slot B-5; launched 12 February 2018
MEO-9	C207	2018-029A	43245	SECM	C29	Slot A-2; launched 30 March 2018
MEO-10	C208	2018-029B	43246	SECM	C30	Slot A-3; launched 30 March 2018
MEO-5	C209	2018-062A	43581	CAST	C23	Slot C-7; launched 29 July 2018
MEO-6	C210	2018-062B	43582	CAST	C24	Slot C-1; launched 29 July 2018
MEO-11	C211	2018-067A	43602	SECM	C26	Slot C-2; launched 25 August 2018
MEO-12	C212	2018-067B	43603	SECM	C25	Slot C-8; launched 25 August 2018
MEO-13	C213	2018-072A	43622	CAST	C32	Slot B-1; launched 19 September 2018
MEO-14	C214	2018-072B	43623	CAST	C33	Slot B-3; launched 19 September 2018
MEO-16	C215	2018-078A	43647	SECM	C35	Slot A-1; launched 15 October 2018
MEO-15	C216	2018-078B	43648	SECM	C34	Slot A-7; launched 15 October 2018
GEO-1	C217	2018-085A	43683	CAST	C59	Launched 1 November 2018
MEO-17	C218	2018-093A	43706	CAST	C36	Slot C-4; launched 19 November 2018
MEO-18	C219	2018-093B	43707	CAST	C37	Slot C-6; launched 19 November 2018
IGSO-1	C220	2019-023B	44204	-	-	Launched 20 April 2019

Table 2. The summaries of the BDS-3 open service signals.

Signal	Signal Component	Carrier Frequency (MHz)	Modulation	Wavelength (cm)	Chip Rate (Mcps)
B1I	-	1561.098	BPSK (2)	19.2	2.046
B1C	B1C_data B1C_pilot	1575.420	BOC QMBOC	19.03	1.023
B2a	B2a_data B2a_pilot	1176.450	BPSK (10)	25.48	10.23
B2b	-	1207.140	QPSK	24.83	10.23
B3I	-	1268.520	BPSK (10)	23.63	10.23

This paper is organized as follows. After this introduction, the TGD correction models of BDS-3 are developed to cover all critical BDS-3 positioning scenarios. In the following section, the experimental data and processing strategies are presented. Then, we analysed the impact of TGD correction on SPP for BDS-2, BDS-3 and the BDS-2 + BDS-3 combination. Finally, the conclusions are given.

2. Methodology

2.1. General Observation Model

The observation equation of code P can be expressed as [25]

$$P_{r,j}^S = \rho_r^S + c \cdot dt_r - c \cdot dt^S + d_{trop} + \gamma_j^S \cdot I_{r,1}^S + \left(d_{r,j} - d_j^S\right) + B_j + \varepsilon_{r,j}^S\left(P_{r,j}^S\right) \quad (1)$$

where r, S and j refer to the receiver, satellite and frequency, respectively; ρ_r^S denotes the geometric distance between the satellite S and the receiver r; c represents the speed of light; dt^S and dt_r are satellite clock offsets and the receiver clock difference between the local time and the system time in seconds, respectively; $I_{r,1}^S$ indicates the slant ionospheric delay on the frequency f_1^S; γ_j^S refers to the frequency-dependent multiplier factor ($\gamma_j^S = \frac{(f_1^S)}{f_j^S})^2$); $d_{r,j}$ and d_j^S represent the uncalibrated code delays (UCDs) at the receiver and satellite end, respectively; B_j is the code biases on frequency j. $\varepsilon_{r,j}^S\left(P_{r,j}^S\right)$ are the noise and multipath error for code observations, respectively.

Currently, the broadcast ephemeris of BDS-3 is divided into two types. One broadcast ephemeris refers to the old signals (B1I and B3I); we call this broadcast ephemeris the old broadcast ephemeris. The other broadcast ephemeris refers to the new signals (B1C and B2a); we call this broadcast ephemeris the new broadcast ephemeris. Compared with the orbit model of BDS-3 with the old broadcast ephemeris, the orbit model of BDS-3 with the new broadcast ephemeris is different, which has been introduced in the BDS-3 ICD [21,25].

Note that the BDS-3 satellite clock is referred to in both the old and new broadcast ephemerides with respect to the B3I signal. Hence, the BDS-3 application using other signals or combined signals differing from the conventional reference signal should apply TGD corrections, which are essential for code-based timing, positioning and ionosphere modelling [10,26]. The correction models of TGD for BDS-3 will be derived and extended to various situations in the next subsection in detail.

2.2. Single-Frequency Users

For single-frequency users, two important issues need to be considered. One issue is the ionospheric delay. Another issue is TGD corrections. Usually, the ionospheric delay is corrected by the Klobuchar model with eight parameters (K8) for B1I, B2I and B3I according to the released public BDS-2 ICD [27] or ionospheric models derived from global ionospheric maps (GIMs) [28]. However, the GIM model does not meet real-time applications; hence, the Klobuchar model is applied in this contribution. With the new signals (B1C and B2a) released by BDS-3, the ionospheric delay correction model does not use

the Klobuchar model with eight parameters; instead the BeiDou global ionospheric delay correction model (BDSGIM) is used. The detailed correction model has been expressed in the BDS-3 ICD [25].

When BDS-3 satellites B1I or B3I are used with the old broadcast ephemeris, B_j can be described as

$$\begin{cases} B_{B1I} = TGD_1 \\ B_{B3I} = 0 \end{cases} \tag{2}$$

where TGD_1 is the "equipment group delay differential" with respect to the B3I signals to maintain signal coherence [29]. When the B3I signal is used, the code bias will not be considered because the broadcast satellite clock offset is based on the B3I signal [20].

When the BDS-3 satellites B1C or B2a are used with the new broadcast ephemeris, B_j can be described as

$$\begin{cases} B_{B1C} = TGD_{B1Cp} \\ B_{B2a} = TGD_{B2ap} \end{cases} \tag{3}$$

where TGD_{B1Cp} is the group delay differential of the B1C pilot component [21] and TGD_{B2ap} is the group delay differential of the B2a pilot component.

2.3. Dual-Frequency Users

For dual-frequency users, the first-order ionospheric delay will be removed by the dual-frequency ionospheric-free combination model. The higher-order ionospheric delay is not considered herein. Although the ionospheric delay is corrected by the ionospheric-free combination model, the TGD corrections still need to be considered for different frequency combinations.

In the BeiDou navigation satellite system open service performance standard (version 2.0), the signals B1I or B1C are recommended for single-frequency services, while the signal combinations B1I/B3I and B1C/B2a are recommended for dual-frequency services [30]. When the B1I/B3I or B1C/B2a ionospheric-free model is used, the code biases $B_{B1I/B3I}$ and $B_{B1C/B2a}$ can be expressed as

$$\begin{cases} B_{B1I/B3I} = \frac{f_{B1I}^2}{f_{B1I}^2 - f_{B3I}^2} TGD_1 \\ B_{B1C/B2a} = \frac{f_{B1C}^2 \cdot TGD_{B1Cp} - f_{B2a}^2 \cdot TGD_{B2ap}}{f_{B1C}^2 - f_{B2a}^2} \end{cases} \tag{4}$$

3. Experimental Data and Processing Strategies

In this experiment, the observation data were selected from six stations provided by iGMAS, namely, BRCH, GUA1, LHA1, WUH1, XIA1, XIA5. The data set is from the days of the year (DOYs) 1 to 41, 2019. The sampling rate is 30 s. All iGMAS stations can track all BDS-3 open signals. The BDS-3 old frequency B1I and B3I broadcast ephemeris are provided by MGEX, and the new frequency B1C and B2a broadcast ephemeris are provided by iGMAS. The data processing strategies of single- and dual-frequency for BDS-2, BDS-3 and BDS-2 + BDS-3 are detailed in Table 3. In Table 3, "non-corr" means code without TGD correction, and "tgd-corr" means code bias correction with TGD parameters in the navigation message. Note that B1I/B3I represents the B1I and B3I ionospheric-free combination SPP model. B1I refers to the single-frequency (B1I) SPP model. The other combination shows similar characteristics. During data processing, the parameter estimation method uses the least squares method, and the troposphere model adopts the Saastamoinen model. The ionospheric delay of the BDS-2 B1I and B3I signals is corrected by the K8 model. With the new signals (B1C and B2a) released by BDS-3, the ionospheric delay correction model adopts the BDSGIM. For dual-frequency data processing, ionospheric delay is used for the dual-frequency ionospheric-free combination. The summaries of the stations are shown in Table 4. Figure 1 shows the distribution of all the stations. The station coordinates in the SINEX file provided by iGMAS (http://112.65.161.230/download/index.php; ftp://222.240.181.170/products/) are used as references values to assess the positioning accuracy [31]. It is noteworthy that the difference

between the iGMAS and IGS station coordinates' precision is at the millimetre level [32,33]. Therefore, the iGMAS station coordinates are sufficient to assess the positioning accuracy.

Table 3. The summaries of the processing strategies.

Model	System	Single-Frequency	Dual-Frequency	Schemes
SPP	BDS-2	B1I, B3I	B1I/B3I	non-corr; tgd-corr
	BDS-3	B1I, B3I, B1C, B2a	B1I/B3I, B1C/B2a	
	BDS-2+BDS-3	B1I, B3I	B1I/B3I	

Table 4. The six selected station information.

Station	Receiver	Antenna
BRCH	CETC-54-GMR-4016	NOV750.R4
GUA1	GNSS-GGR	RINT-8CH
LHA1	CETC-54 GMR-4011	NOV750.R4
WUH1	CETC-54-GMR-4016	LEIAR25.R4
XIA1	GNSS-GGR	RINT-8CH
XIA5	CETC-54-GMR-4011	TRM59900.00

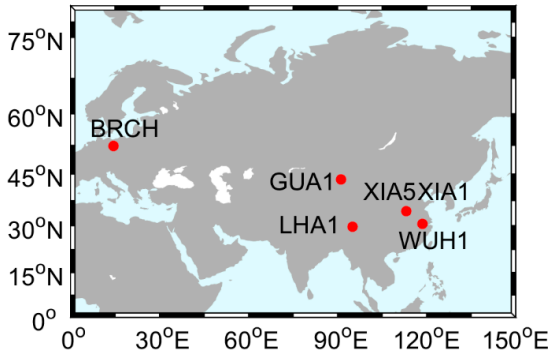

Figure 1. The distribution of the six selected stations from the international GNSS continuous monitoring and assessment system (iGMAS).

4. Validation and Analysis

4.1. BDS-2

We focus first on Figures 2–4 as a typical example, depicting the positioning errors of 21 January 2019 for the east (E), north (N), and up (U) components of B1I and B3I based on BDS-2 SPP with and without TGD correction for the six selected stations. Figures 5 and 6 show the positioning errors of the B1I/B3I ionosphere-free combined E, N, and U components of the BDS-2 SPP at six stations with and without TGD correction on the same day. Note that DOY 21, 2019 (21 January 2019) was randomly selected an example of our study. The other days show similar characteristics, and we do not describe them herein. From the five figures, we can obtain the following four conclusions. First, we can see that Figure 4 is the B3I single-frequency signal with the "non-corr" scheme. As mentioned before, the satellite clocks of BDS-2 in broadcast ephemerides refer to B3I signals. Second, as shown in Figures 2–6, the metre-level positioning accuracy can be achieved with single- and dual-frequency SPP based on the BDS-2. Third, as a point of interest, from Figures 2, 3, 5 and 6, we can see that the significant improvements in the "tgd-corr" scheme are presented. For example, as shown in Figure 2, the horizontal positioning error in the "non-corr" scheme is in the range of −5 m to 5 m, while in "tgd-corr" the scheme is within the range of −2 m to 2 m at the LHA1 station. In Figure 3, the vertical positioning error of the "non-corr" scheme is in the range of −5 m to 5 m, but the result of the "tgd-corr" scheme is within −2 m to 2 m at the LHA1 station. Fourth, by comparing Figures 2, 3, 5 and 6, we can

note that the positioning accuracy of the dual-frequency SPP based on B1I/B3I is even worse than that of the single-frequency based B1I and B3I signals. This phenomenon can be explained by the fact that the noise amplification factor is 3.5 [10] in the B1I/B3I dual-frequency signal based on the SPP scheme.

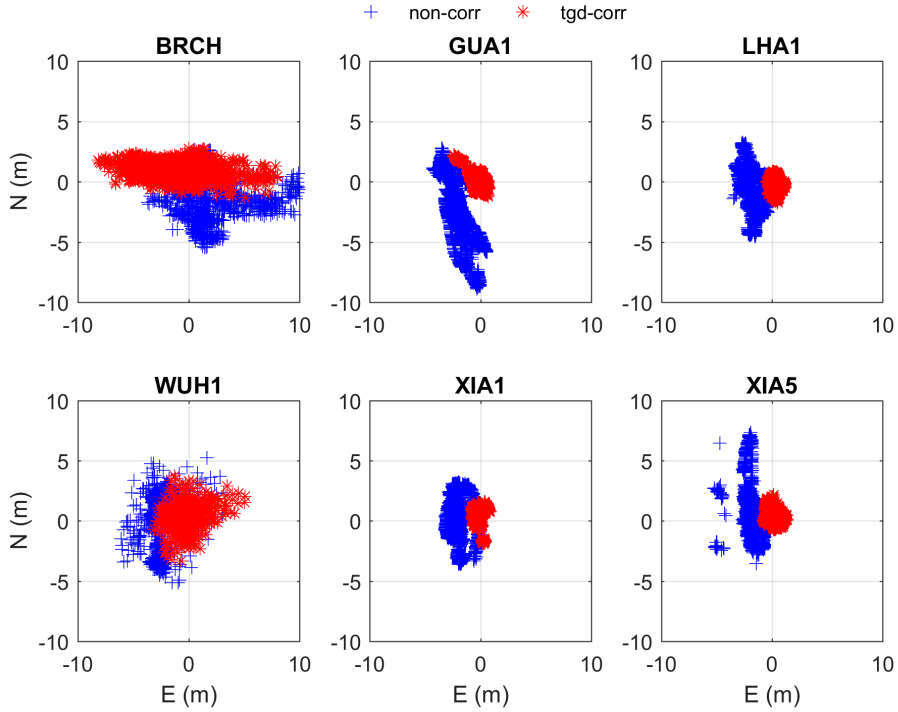

Figure 2. Horizontal positioning error scatter plots of B1I SPP with and without time group delay (TGD) correction at the selected stations. In each plot, the horizontal and vertical axes indicate the East (E) and North (N) components errors, respectively (unit: m).

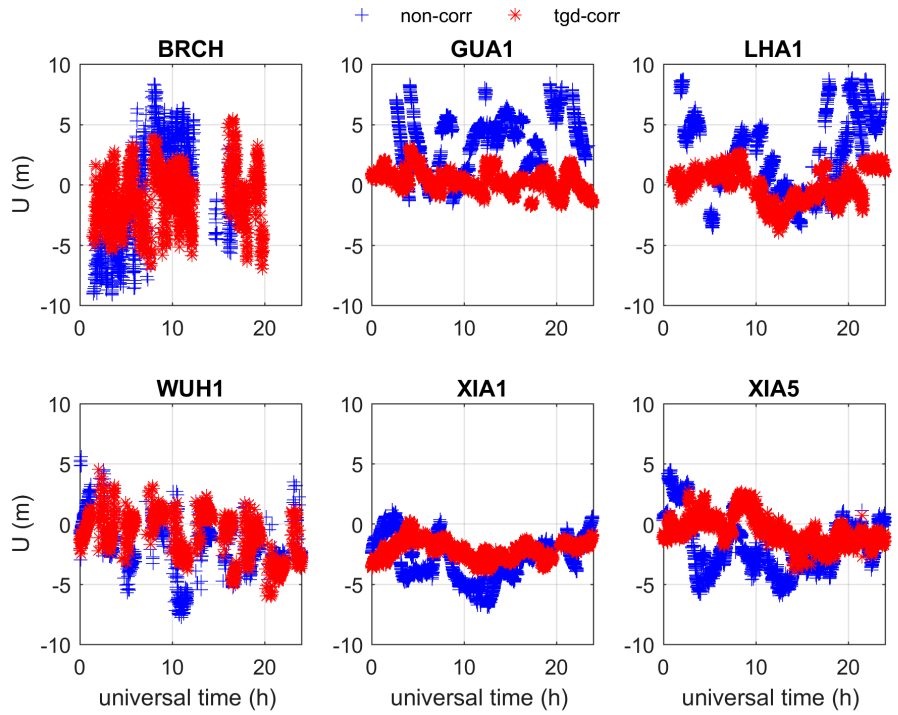

Figure 3. Vertical positioning error scatter plots of B1I SPP with and without TGD correction on the selected stations. In each plot, the horizontal and vertical axes indicate the universal time (h) and the Up (U) component error, respectively (unit: m).

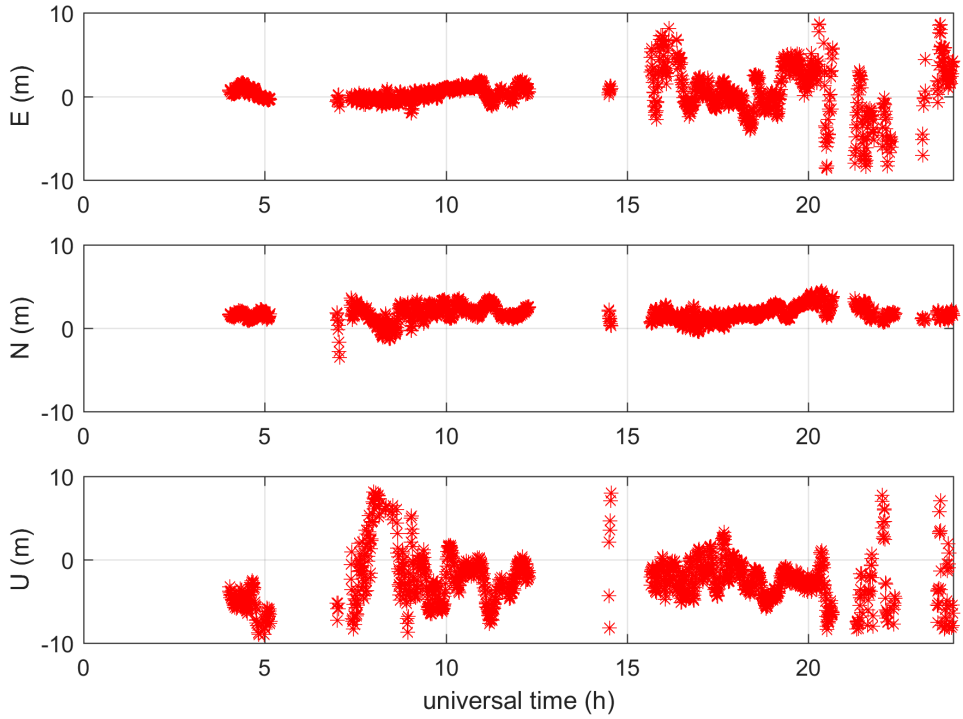

Figure 4. Positioning error scatter plots of B3I SPP without TGD correction for the BRCH station. In each plot, the horizontal axis indicates the universal time (h), and the vertical axes indicates the E, N and U component errors, respectively (unit: m).

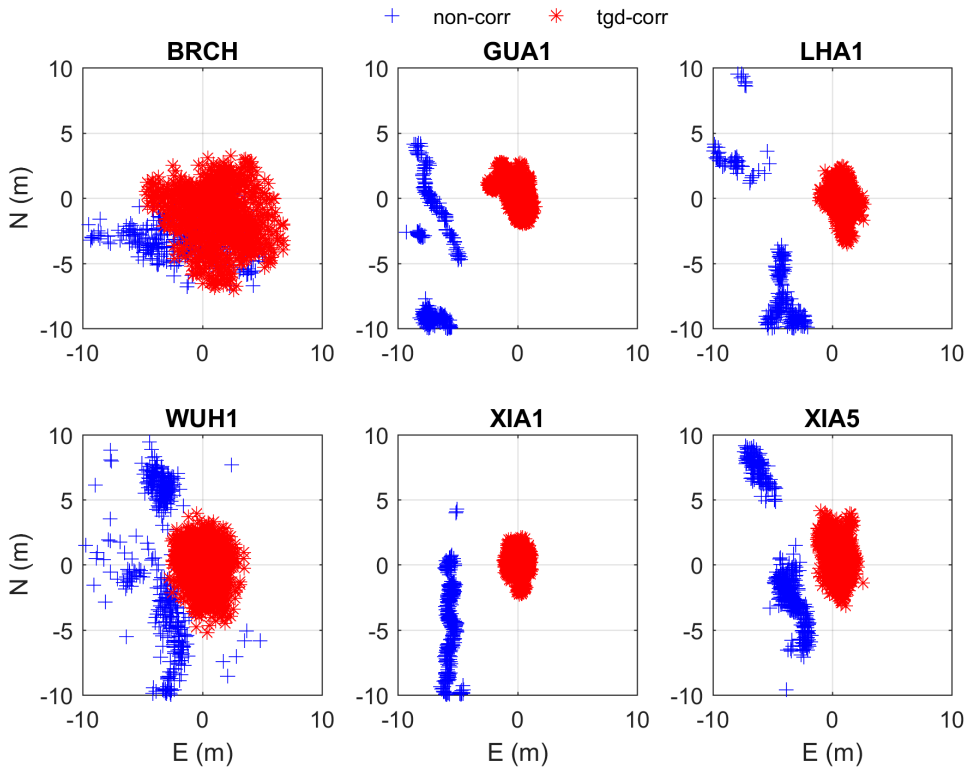

Figure 5. Horizontal positioning error scatter plots of B1I/B3I SPP with and without TGD correction at the selected stations. In each plot, the horizontal and vertical axes indicate the E and N component errors, respectively (unit: m).

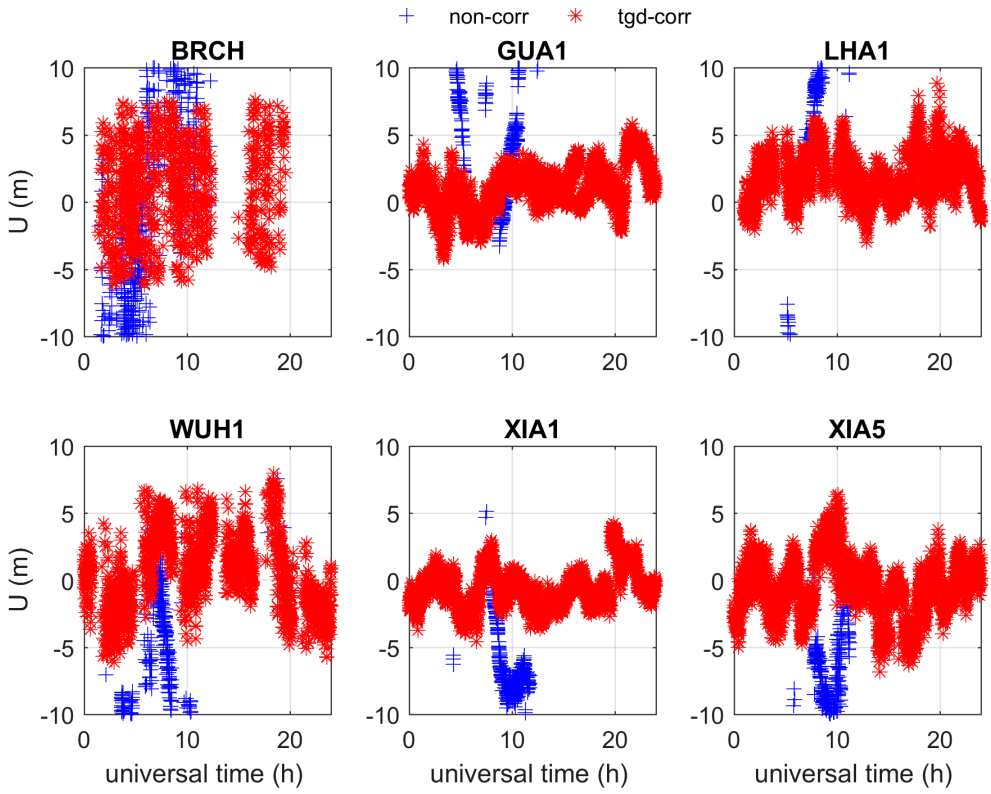

Figure 6. Vertical positioning error scatter plots of B1I/B3I SPP with and without TGD correction at the selected stations. In each plot, the horizontal and vertical axes indicate the universal time (h) and the U component errors, respectively (unit: m).

Figure 7 depicts the box-whisker diagrams of the distribution of three-dimensional (3D) positioning errors in the "tgd-corr" and "non-corr" schemes for the BRCH, GUA1, LHA1, WUH1, XIA1 and XIA5 stations for the period of 41 days. In these diagrams, values are considered outliers if they are less than $Q_1 - 1.5 \cdot IQR$ or greater than $Q_3 + 1.5 \cdot IQR$, where Q_1, Q_3 and IQR denote the first quartile, the third quartile and inter-quartile range of the distribution, respectively. It is intuitively shown in Figure 7 that the number of outliers is very small for all the frequencies at each station. Since the BDS-2 codes are affected by TGD parameters, the "tgd-corr" scheme exhibits better positioning results, which results in reduced positioning errors compared to the "non-corr" scheme. This result is reflected in the distribution of the positioning errors from the "tgd-corr" scheme, exhibiting median and 75th percentile values below 10 m, except at the BRCH station, for all frequencies, as depicted in Figure 7. Furthermore, it can be concluded that the median and 75th percentile values in the Asia-Pacific region are less than those at the BRCH station. We will explain this phenomenon further below. Moreover, the median and 75th percentile values of the "tgd-corr" scheme are less than those of the "non-corr" scheme.

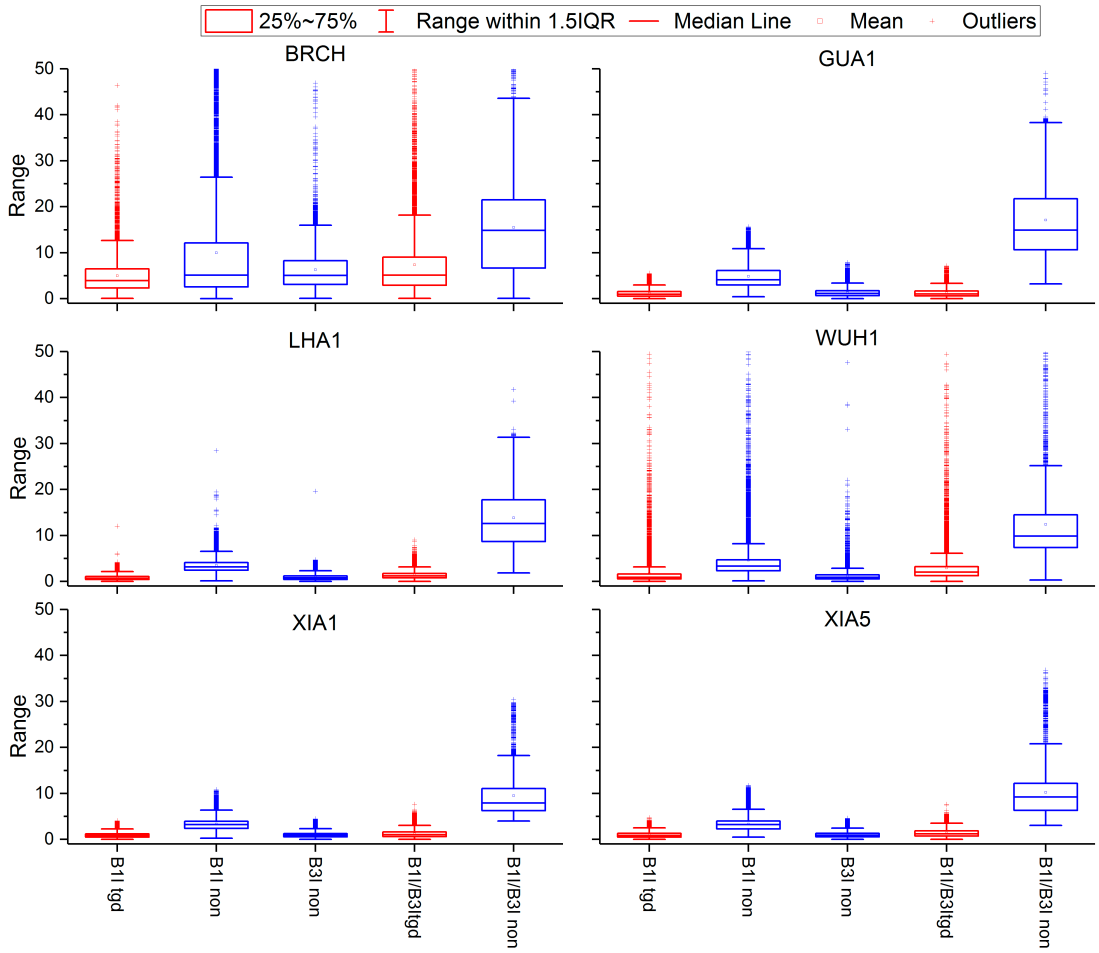

Figure 7. Box-whisker diagrams of the distributions of the three dimensional (3D) positioning errors in the tgd-corr (red) and non-corr (blue) schemes at the BRCH, GUA1, LHA1, WUH1, XIA1 and XIA5 stations for the 41-day period (tgd: tgd-corr, non: non-corr) using the regional BeiDou system (BDS-2) satellites. The box heights and the bars inside the boxes denote the inter-quartile ranges (IQRs) and the medians of the distributions, respectively. The whiskers' lengths represent the maximum and minimum values of distributions (unit: m). Outliers are identified with plus signs (see the text).

To analyse the BDS-2 positioning accuracy from different schemes based on the SPP more clearly, the root mean square (RMS) of the single- and dual-frequency SPP are calculated, and we plot the RMS of each day for the different stations (Figure 8). In addition, the improvements in the E, N, U components of the "tgd-corr" scheme compared to the "non-corr" scheme at different stations are shown in Figure 9. In Figure 9, we first obtain the mean RMS values of the 41-day SPP solutions at each station. The improvements from the "tgd-corr" scheme are then calculated and compared to those from the "non-corr" scheme. In addition, the mean values at the six stations are summarized in Table 5. Note that the outliers appearing in SPP are treated as follows. The pre-test and post-test residuals are checked in our program. Observations are deleted when the absolute value of residual is greater than 30 m. The main conclusion to be drawn from Figures 8 and 9, in conjunction with Table 5, is straightforward. It is obvious that both the single- and dual-frequency SPP of the BDS-2 can achieve metre-level positioning accuracy. As we can see from Figure 8, the results based on B1I and B1I/B3I SPP without TGD correction deviate from the true position. From Figure 9, we can conclude that the accuracy of B1I/B3I- or B1I- based SPP with TGD correction, in addition to that at the BRCH station, in the E and N components increased by more than 50%, and the U component increased in the range of 25% to 50%. The reason for the slight improvement at the BRCH station is that BRCH is in Europe, so the number of observed BDS-2 satellites is relatively small, which results in

an unsatisfactory equation structure. We can further explain from Figure 10, which shows the average global position dilution of precision (PDOP) on DOY 10, 2019, with an elevation cut-off angle of 5°. The PDOP is a spatial geometric intensity factor of the satellite distribution; the better the general satellite distribution is, the smaller the PDOP value. From Figure 10, we can conclude that the BDS-2 PDOP presents obvious regional characteristics. The PDOP value of the BRCH station in Europe is greater than that of the Asia-Pacific region where the other stations are located, which support our previous findings. In addition, some BDS-2 satellites have a high degree of noise at lower elevation angels in the European region. Hence, the TGD correction of the BDS-2 system has less effect on the accuracy of the BRCH station. From the average RMS values of the six stations in Table 5, compared with the "non-corr" scheme of the B1I-based solutions, the positioning accuracy of the "tgd-corr" scheme is notably improved by 52.4% from 2.69 m to 1.28 m and by 57.8% from 2.3 m to 0.97 m in the horizontal directions. In addition, for the vertical direction, the B1I-based positioning results are improved by 45.6% from 4.08 m to 2.22 m. Interestingly, the B3I-based positioning results are not affected by the TGD parameter because the satellite clocks of BDS-2 in the broadcast ephemeris refer to the B3I signal. Under the "tgd-corr" scheme, the RMS values of single- and dual-frequency signals for the horizontal and vertical components are 1 m–2 m. For the "tgd-corr" scheme, the RMS values of the B1I/B3I combination are significantly reduced by 70.1% from 5.36 m to 1.6 m, by 74.2% from 5.12 m to 1.32 m and by 47.4% from 5.67 m to 2.98 m for the E, N and U components, respectively.

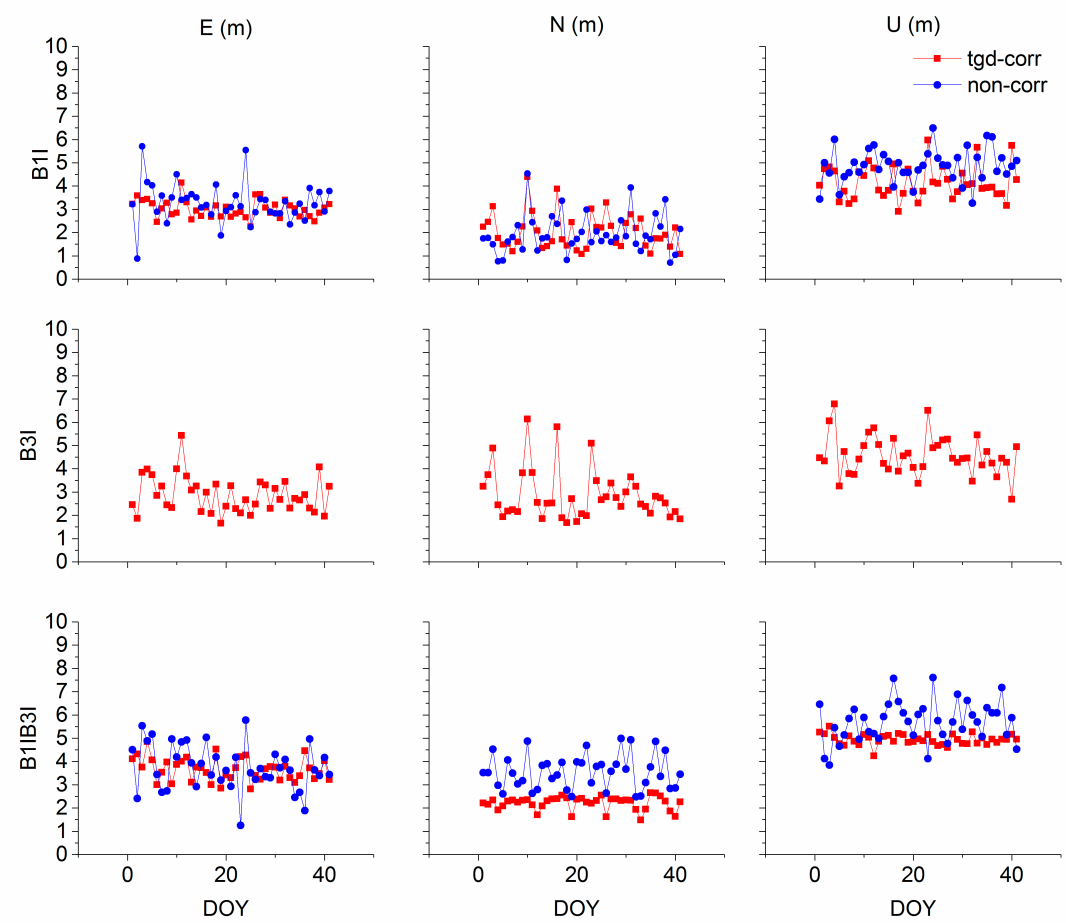

Figure 8. Daily RMS values of BDS-2 with different schemes for the BRCH station.

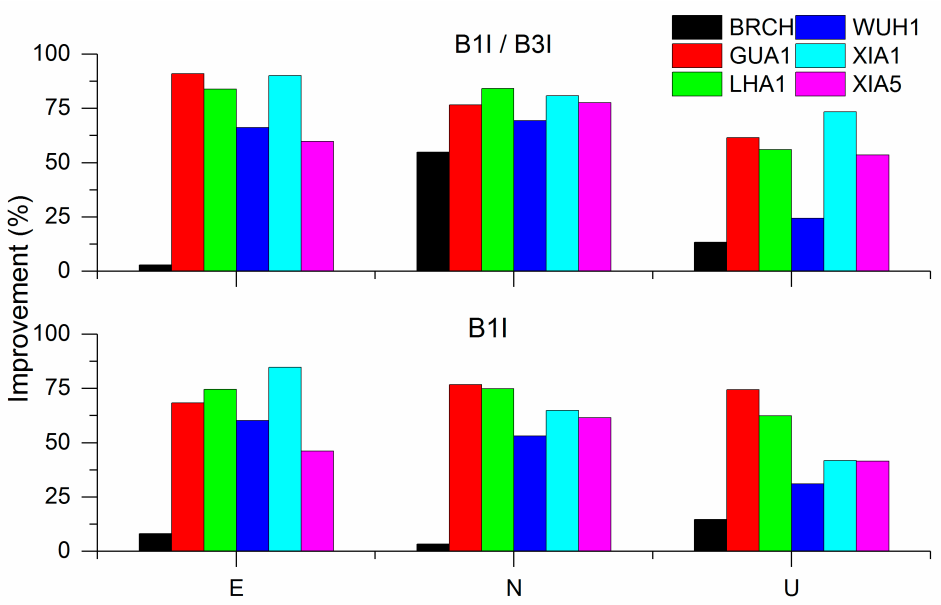

Figure 9. Improvements in the E, N, and U components of the "tgd-corr" scheme compared to the "non-corr" scheme at different stations. Note that the mean RMS of 41 days at each station with and without TGD correction is first obtained. The improvement from the "tgd-corr" scheme is then calculated and compared to that from the "non-corr" scheme.

Table 5. The mean root mean square (RMS) values of the six selected stations SPP solutions using 41-day observations with and without TGD correction in different BDS-2 frequency combinations (m).

	Scheme	B1I	B3I	B1I/B3I
E	tgd-corr	1.28	-	1.60
	non-corr	2.69	1.27	5.36
	Improvement (%)	52.4	-	70.1
N	tgd-corr	0.97	-	1.32
	non-corr	2.30	1.12	5.12
	Improvement (%)	57.8	-	74.2
U	tgd-corr	2.22	-	2.98
	non-corr	4.08	2.75	5.67
	Improvement (%)	45.6	-	47.4

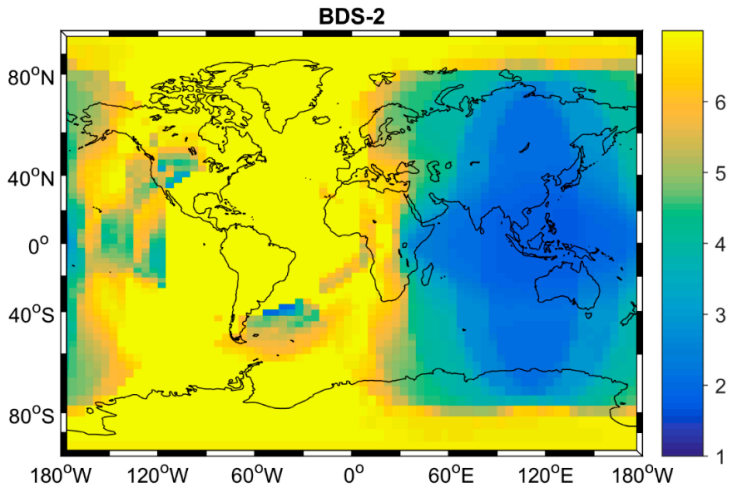

Figure 10. Average global PDOP of BDS-2 on day of the year (DOY) 10 2019 with an elevation cut-off angle of 5°.

4.2. BDS-3

Figures 11–17 present the horizontal and vertical positioning error scatters plots of the BDS-3 single-frequency SPP, with and without TGD correction, from 21 January 2019 for the six stations. It should be explained that the data are discontinuous because of the lack of observational data in the figures. In addition, we mentioned before that the pre-test and post-test residuals will be checked in our program, and the observations will be deleted when the absolute value of the residual is greater than 30 m. Considering all seven figures, there are three findings highlighted here. First, simultaneously considering Figures 13–16, it can be seen that the positioning accuracy values of the B1C and B2a signals have improved significantly with the "tgd-corr" scheme. We can conclude that the TGD parameters need to be modified in the B1C-and B2a-based positioning. As mentioned in the ICD file, the TGD of B1C is the group delay differential between the B1C pilot component and the B3I signal, and the TGD of B2a is the group delay differential between the B2a pilot component and the B3I signal. Second, both the old signals and the new signals, in the case of correcting the TGD parameters, can achieve the metre-level positioning accuracy. Third, we can clearly see that the "tgd-corr" scheme results in a significant improvement compared to the "non-corr" scheme positioning results in the E, N and U components. Taking the B1C signal of the LHA1 station as an example, in Figures 13 and 14, the horizontal and vertical positioning errors are within the range of −5 m to 5 m after the correction of the TGD parameters, and those from the uncorrected TGD parameters range from −10 m to 10 m.

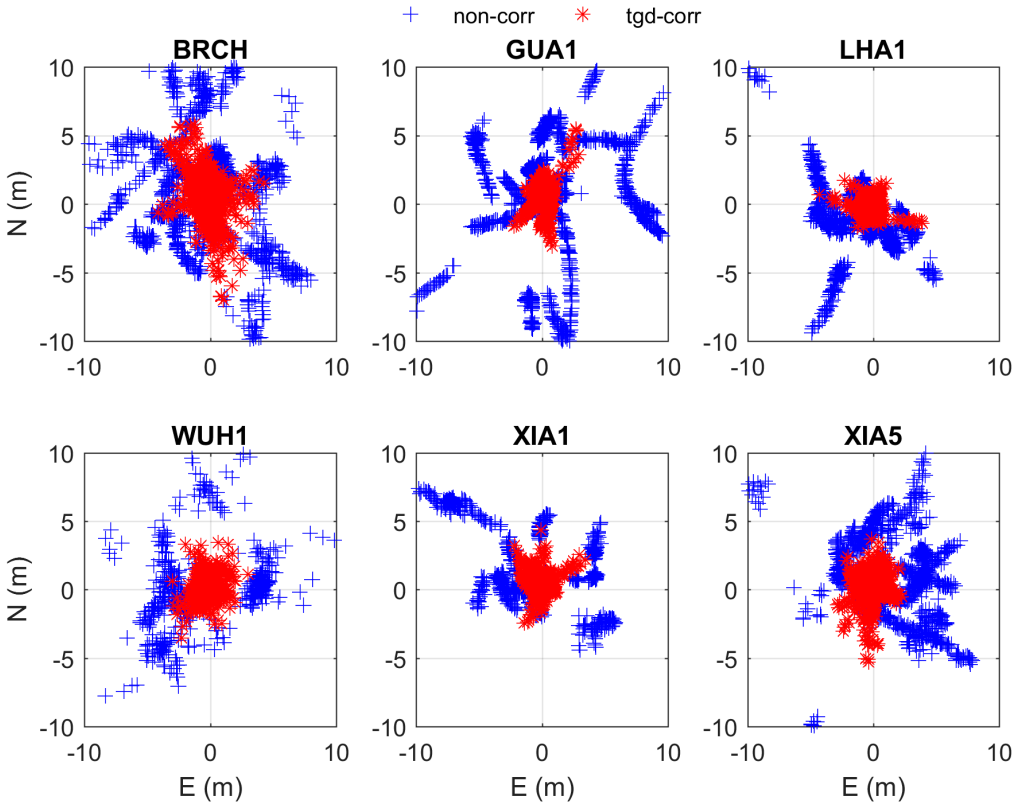

Figure 11. Horizontal positioning error scatter plots of B1I SPP with and without TGD correction for the six selected stations. In each plot, the horizontal and vertical axes indicate the E component error and the N component error, respectively (unit: m).

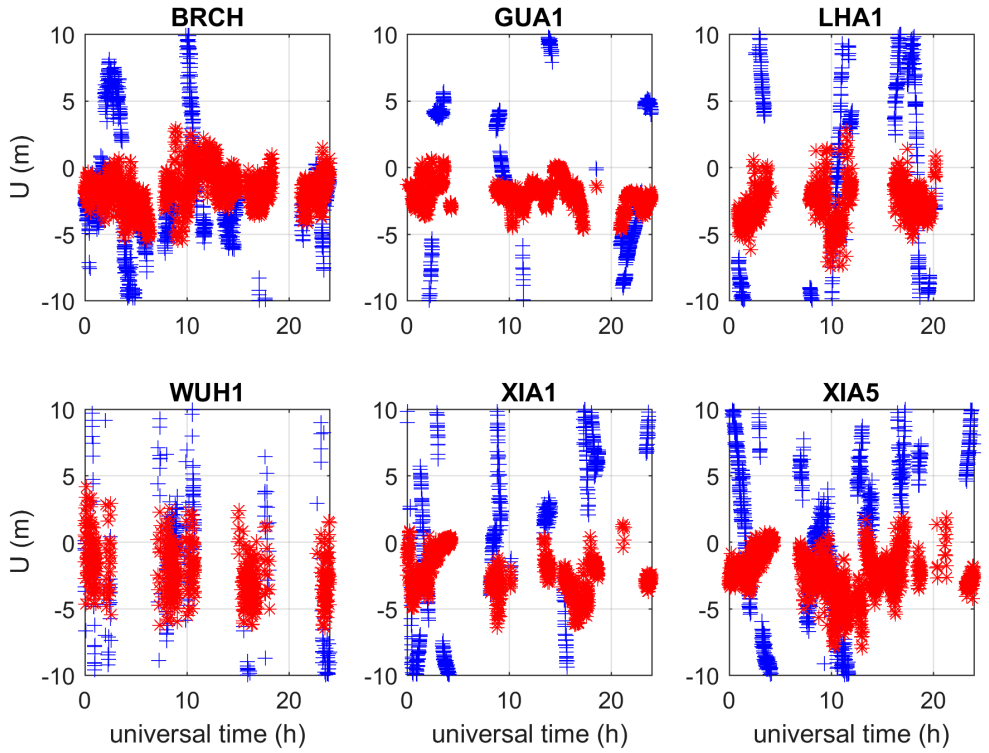

Figure 12. Vertical positioning error scatter plots of B1I SPP with and without TGD correction for the six selected stations. In each plot, the horizontal and vertical axes indicate the universal time (h) and the U component error, respectively (unit: m).

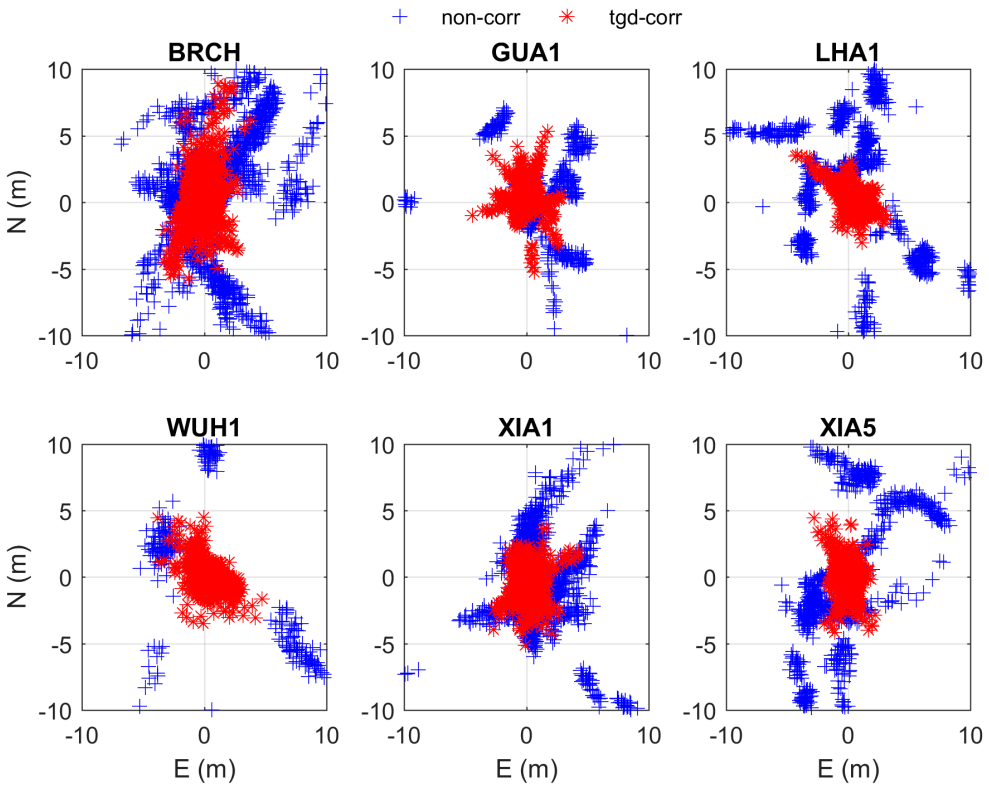

Figure 13. Horizontal positioning error scatter plots of B1C SPP with and without TGD correction for the six selected stations. In each plot, the horizontal and vertical axes indicate the E component error and the N component error, respectively (unit: m).

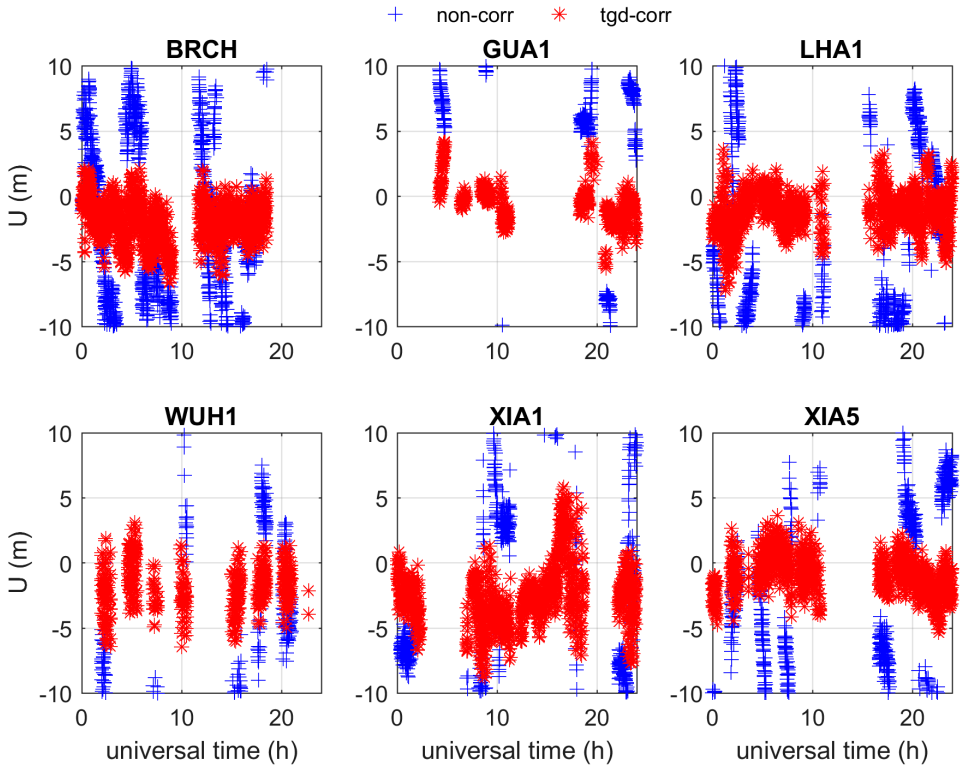

Figure 14. Vertical positioning error scatter plots of B1C SPP with and without TGD correction for the six selected stations. In each plot, the horizontal and vertical axes indicate the universal time (h) and the U component error, respectively (unit: m).

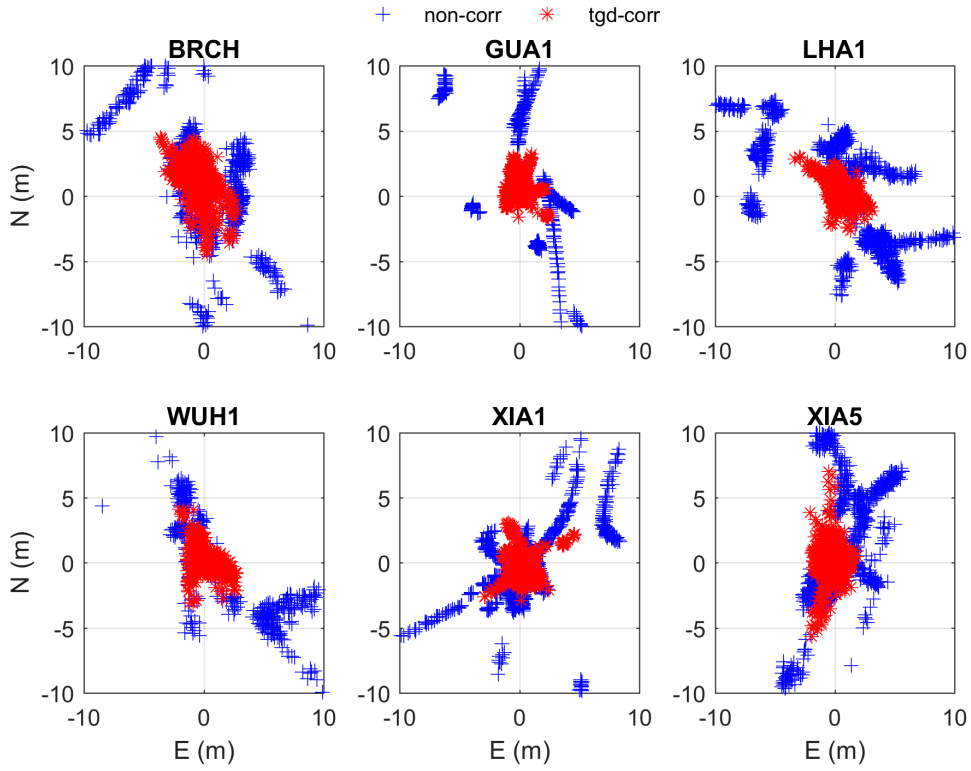

Figure 15. Horizontal positioning error scatter plots of B2a SPP with and without TGD correction for the six selected stations. In each plot, the horizontal and vertical axes indicate the E component error and the N component error, respectively (unit: m).

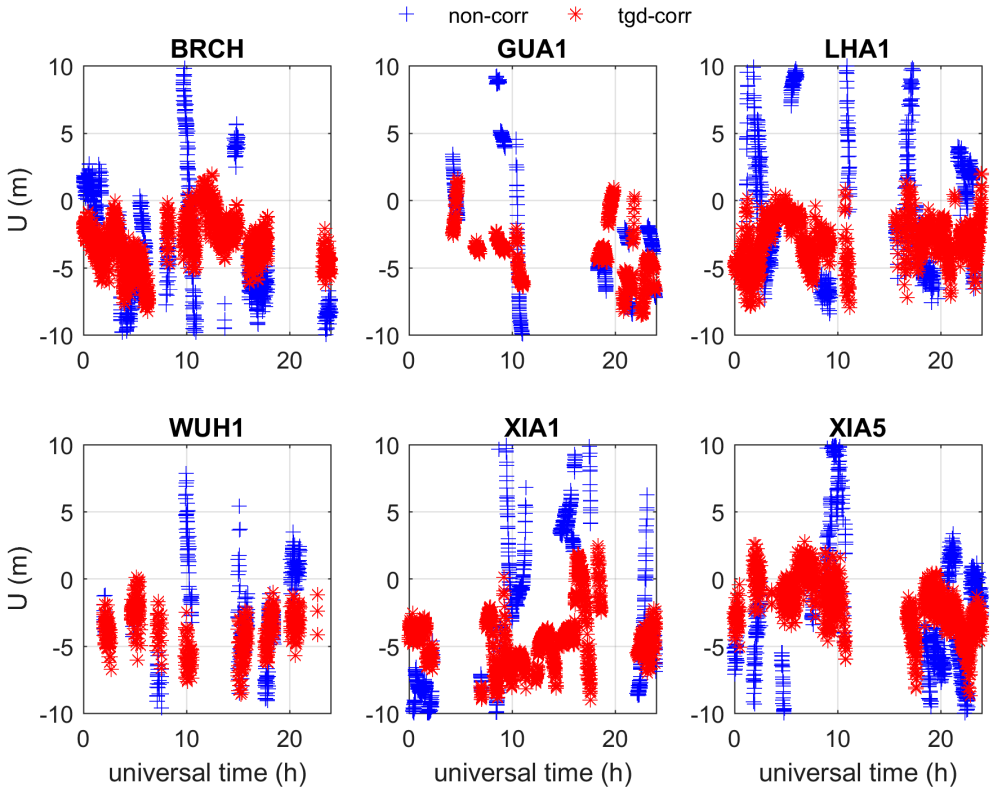

Figure 16. Vertical positioning error scatter plots of B2a SPP with and without TGD correction for the six selected stations. In each plot, the horizontal and vertical axes indicate the universal time (h) and the U component error, respectively (unit: m).

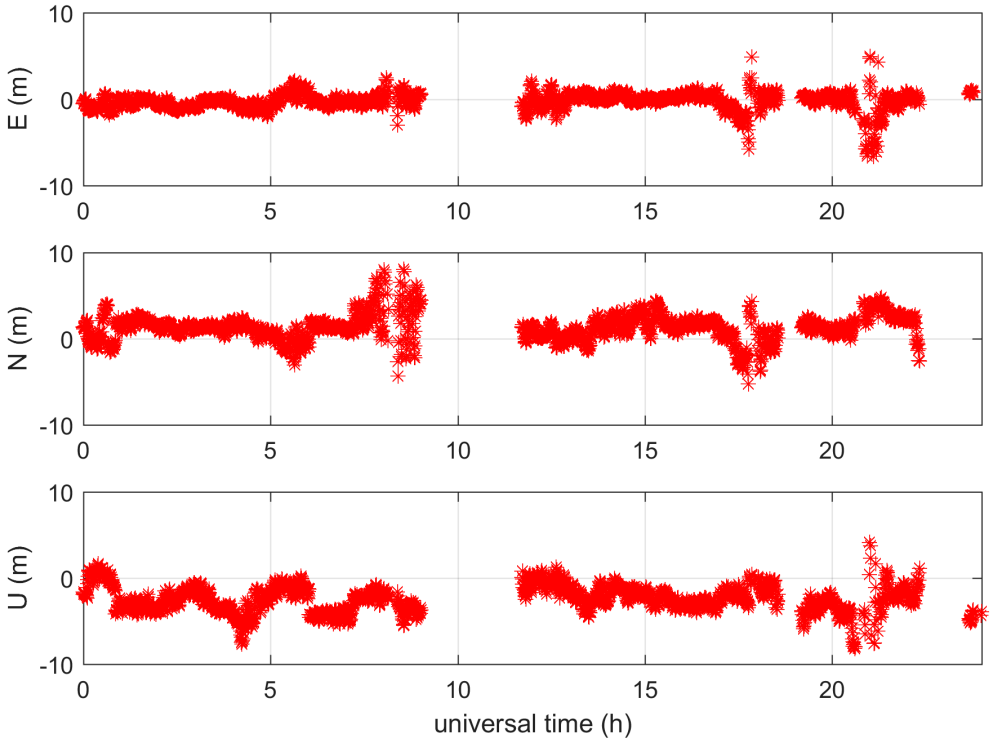

Figure 17. Vertical positioning error scatter plots of B3I SPP without TGD correction for the BRCH station. In each plot, the horizontal axis is the universal time (h) and the vertical axes indicate the errors of the E, N and U components (unit: m).

We now turn to Figures 18–21, in which the four panels separately show the horizontal and vertical positioning error scatter plots of BDS-3 B1I/B3I- and B1C/B2a-based SPP from 21 January 2019. As we can see from the four figures, both the old and new signals of BDS-3 dual-frequency SPP can reach metre-level positioning accuracy. We focus on the B1C/B2a-based positioning errors shown in Figures 20 and 21. The positioning error from the "tgd-corr" scheme is within ±5 m, and the positioning error from the "non-corr" scheme is within ±10 m in the E, N and U components. Combined with Figures 17 and 18, we can still conclude that the TGD correction effect of the new signal is obviously similar to that of the old signal. Interestingly, we note that the noise in the dual-frequency positioning errors is greater than that in the single-frequency positioning errors. We surmise that this finding may be attributed to the fact that noise is magnified in the dual-frequency SPP scheme [10].

Figure 22 shows box-whisker diagrams of the distributions of the positioning errors in the tgd-corr and non-corr schemes for the six stations for the 41-day period. The outliers, first quartile, third quartile and inter-quartile range in the distribution in the figure are as stated before. There are three findings highlighted here. First, it is obvious in the figure that the number of outliers at each station is very small, which further proves that positioning using BDS is reliable. Second, unlike for BDS-2, the positioning errors for all stations are basically similar; thus, we can conclude that BDS-3 eliminated the regional limitation characteristics of BDS-2. Third, including the BRCH station, the medians and 75th percentiles from the "tgd-corr" scheme at all stations is less than 10 m. For the "non-corr" scheme, the medians and 75th percentiles are much larger than those from the "tgd-corr" scheme, which proves that the TGD parameters need to be corrected for BDS-2 positioning.

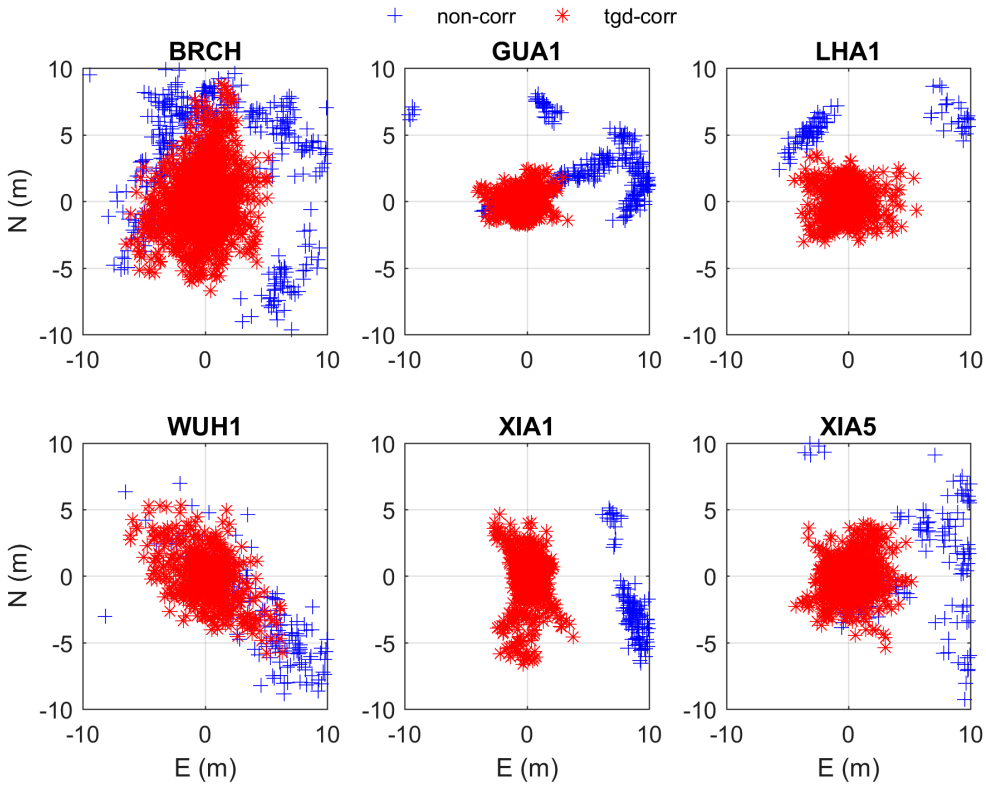

Figure 18. Horizontal positioning error scatter plots of B1I/B3I SPP with and without TGD correction for the six selected stations. In each plot, the horizontal and vertical axes indicate the E component error and the N component error, respectively (unit: m).

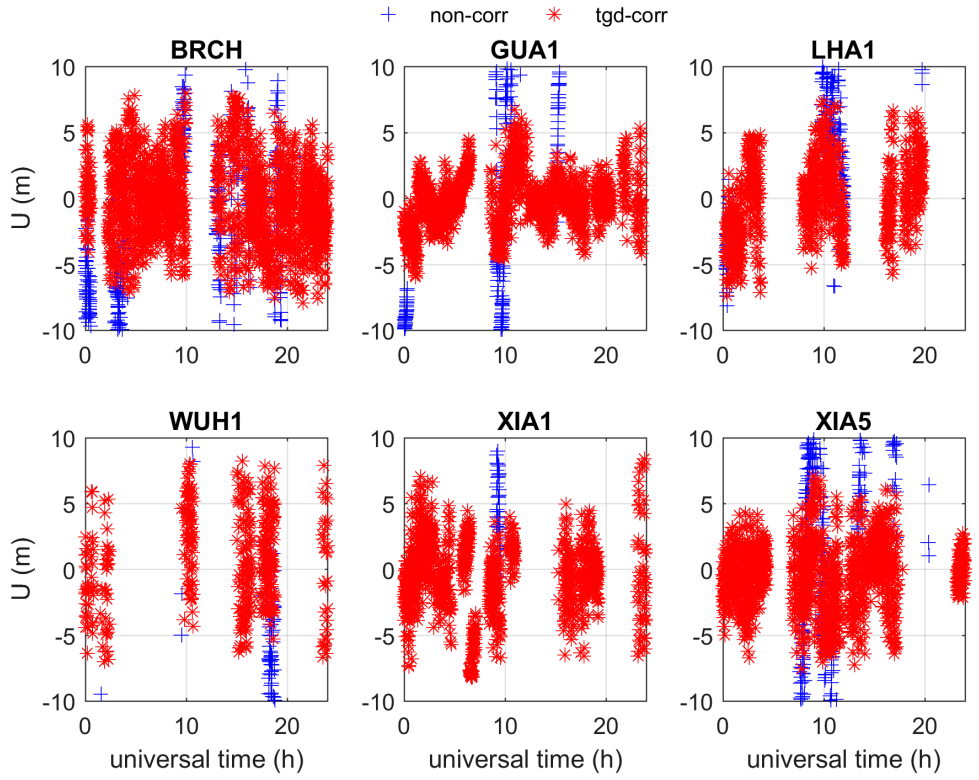

Figure 19. Vertical positioning error scatter plots of B1I/B3I SPP with and without TGD correction for the six selected stations. In each plot, the horizontal and vertical axes indicate the universal time (h) and the U component error, respectively (unit: m).

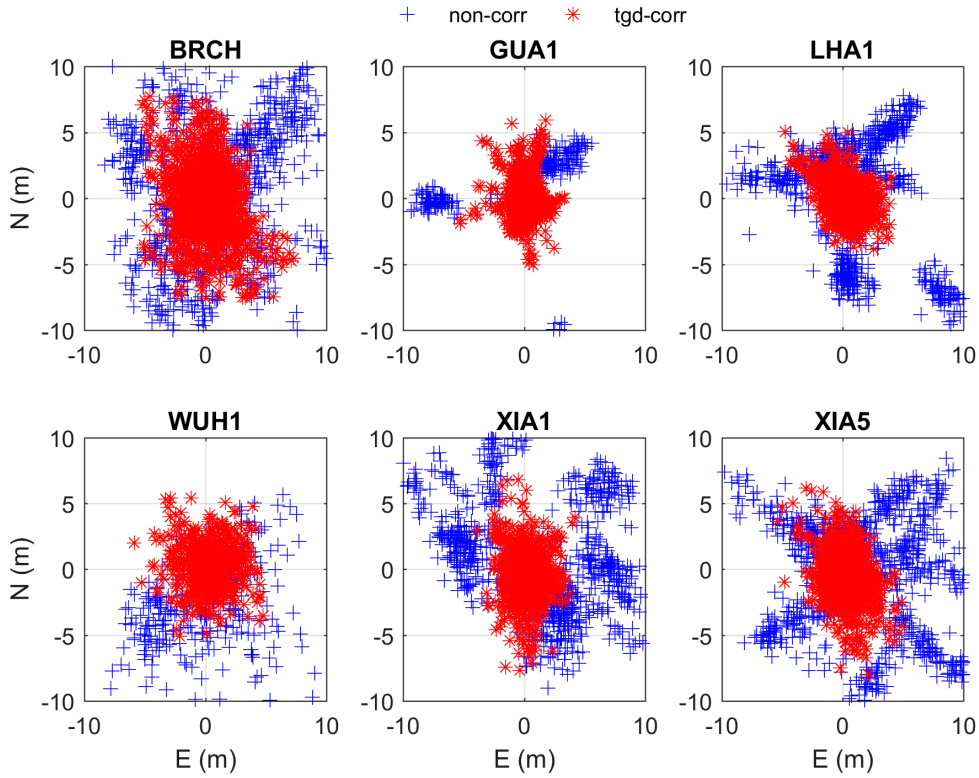

Figure 20. Horizontal positioning error scatter plots of B1C/B2a SPP with and without TGD correction for the six selected stations. In each plot, the horizontal and vertical axes indicate the E component error and N component error, respectively (unit: m).

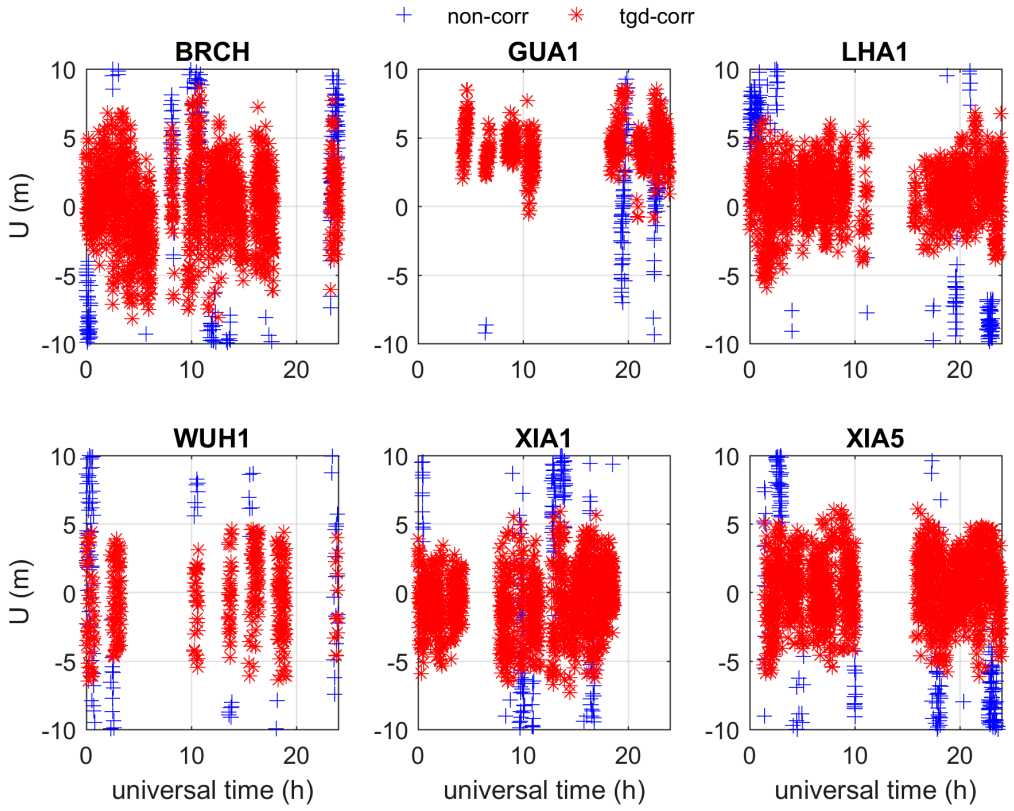

Figure 21. Vertical positioning error scatter plots of B1C/B2a SPP with and without TGD correction for the six selected stations. In each plot, the horizontal and vertical axes indicate the universal time (h) and the U component error, respectively (unit: m).

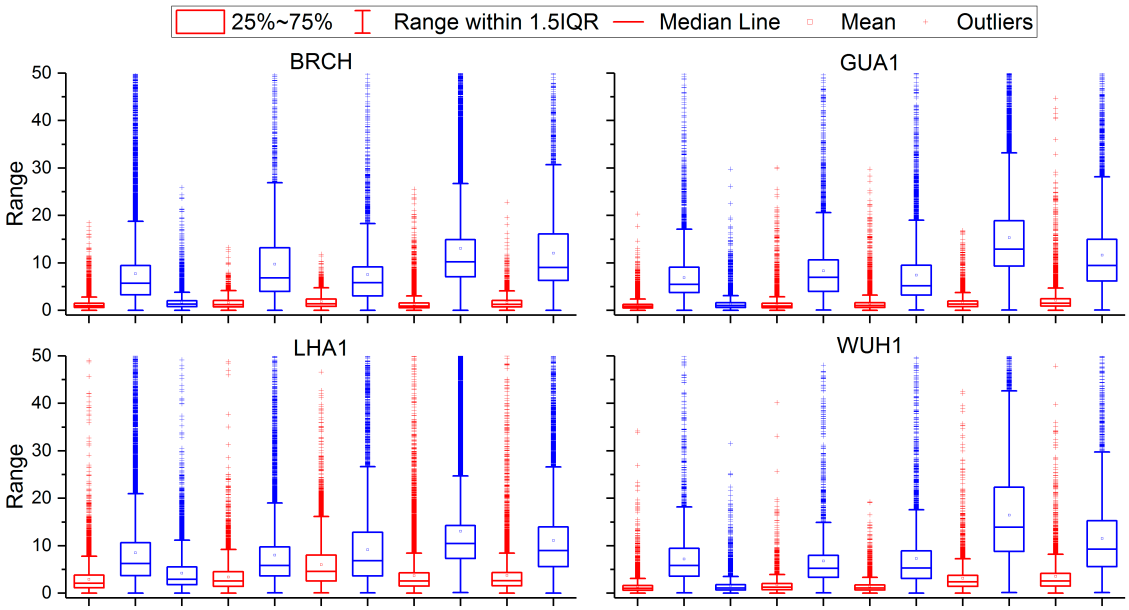

Figure 22. *Cont.*

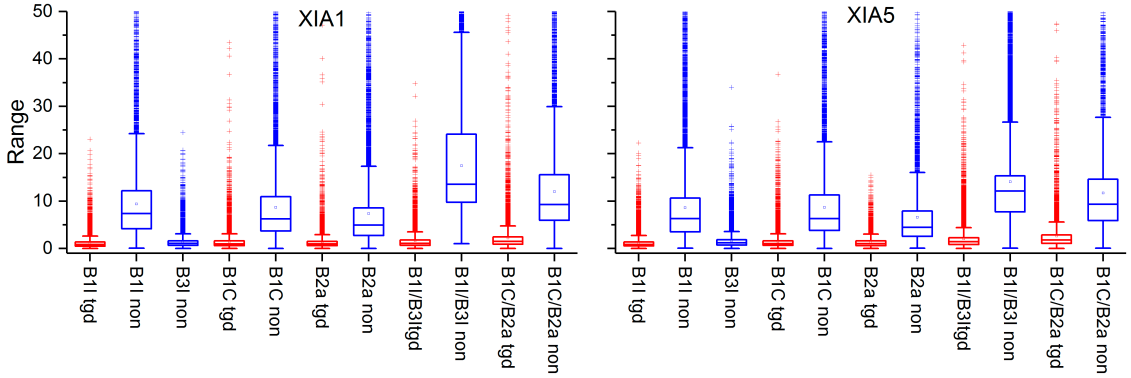

Figure 22. Box-whisker diagrams of the distributions of the 3D positioning errors in the tgd-corr (red) and non-corr (blue) schemes at the BRCH, GUA1, LHA1, WUH1, XIA1 and XIA5 stations for the 41-day period (tgd: tgd-corr, non: non-corr) using the BDS-3 satellites. The box heights and the bars inside the boxes denote the IQRs and medians of the distributions, respectively. The whiskers' lengths represent the maximum and minimum values of the distributions (unit: m). Outliers are identified with plus signs (see text).

To further quantify the positioning accuracy, we give the RMS values for the daily single- and dual-frequency positioning errors with and without TGD correction for the BRCH station, displayed in Figures 23 and 24. In the two figures, it is clearly shown that both the single- and dual-frequency positioning accuracy values with TGD correction are better than those without TGD correction. The positioning accuracy of B1C- and B2a-based BDS-3 SPP is similar to that of B1I- and B3I-based SPP. The above results can be further demonstrated in Figure 25, showing the improvement in the E, N and U components from the "tgd-corr" scheme compared to that from the "non-corr" scheme at different stations. First, we consider the single-frequency positioning accuracy. Taking the B1C signal as an example, the horizontal positioning accuracy with the "tgd-corr" scheme is more than 50% higher than that with the "non-corr" scheme, and the vertical positioning accuracy is improved by more than 25%. The B1I- and B2a-based SPP results at other stations show similar features to those of the B1C signal; we will not describe them in detail herein. Second, for the positioning accuracy of B1C/B2a- and B1I/B3I-based SPP, the horizontal positioning accuracy based on the "tgd-corr" scheme compared to the "non-corr" scheme improved in the range of 33.93% to 85.08%, and the vertical positioning accuracy was improved in the range of 30.12% to 59.19%. We also calculated the means of the RMSs at different frequencies and different schemes for 41 days at the six stations (Table 6). The empirical analysis of the obtained results yielded three conclusions. First, the signal- and dual-frequency SPP solutions without the TGD correction present the systematic error. Compared with the "non-corr" scheme, the accuracy in B1I SPP is improved with the TGD correction by approximately 68.0%, 69.2% and 49.2% in the N, E and U components, respectively. The positioning errors of B1C SPP with the "tgd-corr" scheme are reduced by 64.8% from 1.18 m to 3.35 m and by 64.4% from 1.48 m to 4.16 m and by 51.2% from 2.91 m to 5.96 m in the E, N and U components, respectively. In the "tgd-corr" scheme, the RMS values of B2a SPP are significantly reduced by 60.2% from 2.84 m to 1.13 m, by 55.4% from 3.59 m to 1.60 m and by 19.8% from 5.09 m to 4.18 m in the E, N and U components, respectively. Likewise, compared with the "non-corr" scheme, the RMS of B1I/B3I SPP is reduced by 75% and 71% in the horizontal components, and the positioning accuracy can reach 1 m–2 m after TGD correction, and the vertical component is reduced by 45.4%, from 5.42 m to 2.96 m. The accuracy of B1C/B2a SPP with the "tgd-corr" scheme is improved by 66.1% and 62.1% on the horizontal components, the N and E can reach 1.66 m and 1.85 m by correcting the TGD parameters, respectively, and the vertical component is improved by 43.3%, from 6.31 m to 3.58 m. Second, we focus on the new signals from BDS-3. We observe that the positioning accuracy of the new signals is analogous to that of the old signals of BDS-3. Both the new and old signals can achieve a positioning accuracy similar to that of BDS-2. However, BDS-2 provides regional location services, while BDS-3 provides global location services. Third, we note that

the positioning accuracy of the dual-frequency SPP is even worse than that of single-frequency: This result is affected by the fact that the dual-frequency observation noise is significantly enlarged due to different factors, including the TGD parameter error.

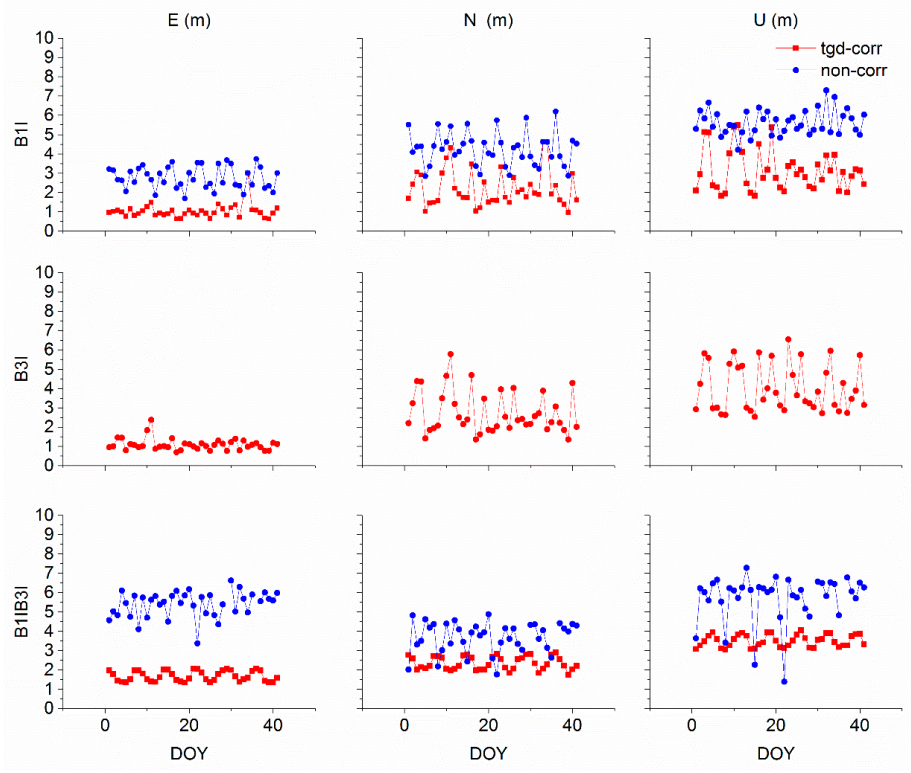

Figure 23. Daily RMSs of old signals from BDS-3 with and without TGD correction for the BRCH station.

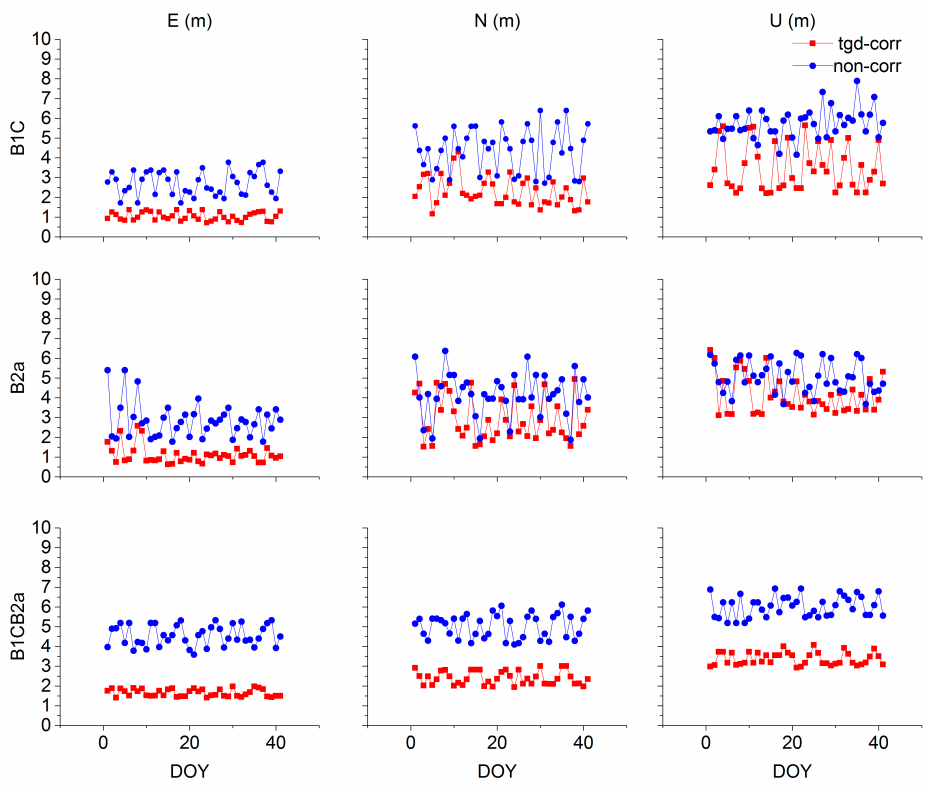

Figure 24. Daily RMSs of the new signals from BDS-3 with and without TGD correction for the BRCH station.

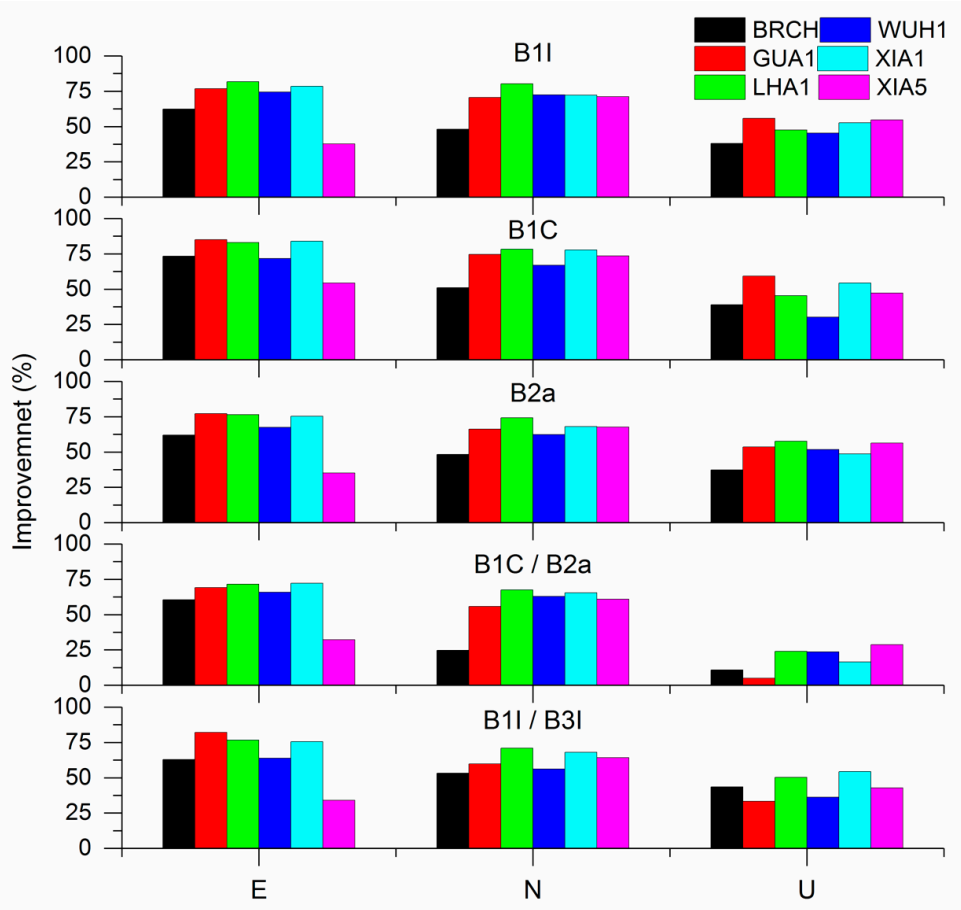

Figure 25. Improvements in the E, N and U components from the "tgd-corr" scheme compared to those from the "non-corr" scheme for different stations. Note that the 41-day mean RMS at each station with and without TGD correction is obtained first. The improvements from the "tgd-corr" scheme is then calculated and compared to those from the "non-corr" scheme.

Table 6. The 41-day mean RMS values of the SPP solutions with/without TGD correction in different BDS-3 frequency combinations from the six selected stations (m).

	Scheme	B1I	B3I	B1C	B2a	B1I/B3I	B1C/B2a
E	tgd-corr	1.08	-	1.18	1.13	1.53	1.66
	non-corr	3.38	1.15	3.35	2.84	6.13	4.89
	Improvement (%)	68.0	-	64.8	60.2	75.0	66.1
N	tgd-corr	1.29	-	1.48	1.60	1.67	1.85
	non-corr	4.19	1.57	4.16	3.59	5.76	4.88
	Improvement (%)	69.2	-	64.4	55.4	71.0	62.1
U	tgd-corr	2.73	-	2.91	4.18	2.96	3.58
	non-corr	5.37	3.54	5.96	5.09	5.42	6.31
	Improvement (%)	49.2	-	51.2	19.8	45.4	43.3

We now turn to Figure 26, which depicts the code residual scatters at the BRCH station with different schemes, with each colour representing different satellites. We see that there is a clear system bias in the code residual of each satellite with the "non-corr" scheme. It is noteworthy that there is no significant system bias with the "tgd-corr" scheme; thus, this finding further verifies that the TGD of the old and new signals from BDS-3 need to be modified. Comparing the two schemes, it can be found that the data from the "non-corr" scheme are less than the data from the "tgd-corr" scheme, possibly because the code residuals are too large during the calculation process. We focus on Figure 27, which shows the average global PDOP on DOY 10 2019, with an elevation cut-off angle of 5°. Compared with

Figure 10, we can clearly conclude that the global PDOP value for BDS-3 is less than that for BDS-2, which further supports our previous conclusions. The number of BDS-3 satellites has increased in Europe, making the correction of the TGD parameters more significant for the BRCH stations. With the rapid development of BDS-3, it now has a global network of 20 satellites and provides global services. We also expect that a better performance from BDS-3 can be reached when the global system is completed in 2020.

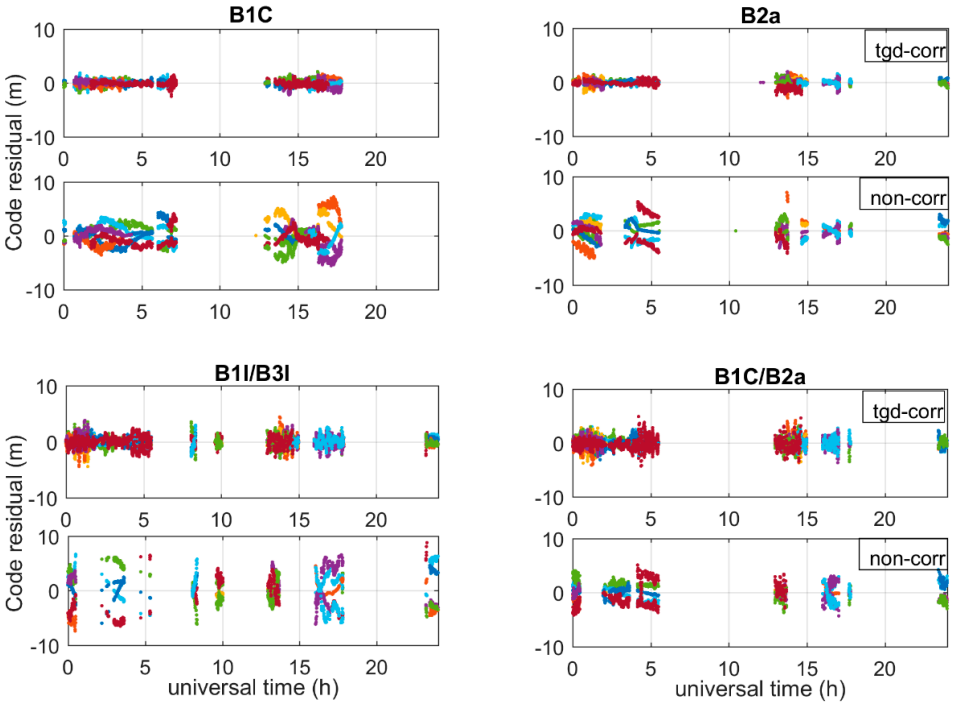

Figure 26. Code residual scatter plots for the BRCH station with/without TGD correction. In each plot, the horizontal and vertical axes indicate the universal time (h) and the code residual, respectively (unit: m).

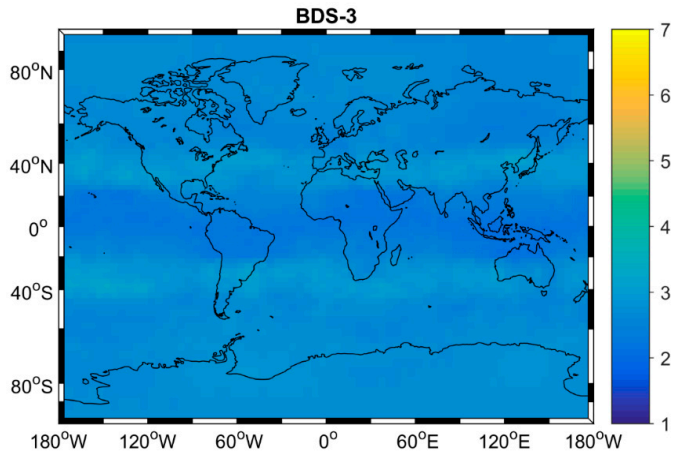

Figure 27. Average global PDOP of BDS-3 on DOY 10 2019, with an elevation cut-off angle of 5°.

4.3. BDS2 + BDS-3

With the previous validation, we can conclude that the TGD parameters of the B1I, B1C and B2a signals need to be corrected. Therefore, for the BDS-2 + BDS-3 combination, we give only the positioning results with the TGD correction in this subsection. Figures 28–31 display the horizontal and vertical positioning error scatter plots for B1I and B3I SPP on 21 January 2019. The positioning errors in the B1I/B3I signal from a single day are described in Figures 32 and 33. From the positioning

results, it can be concluded that the positioning accuracy of the BDS-2 + BDS-3 combined system is higher than that of BDS-2 or BDS-3 because the increase in the number of BDS-3 satellites has made up for the regional limitations of BDS-2.

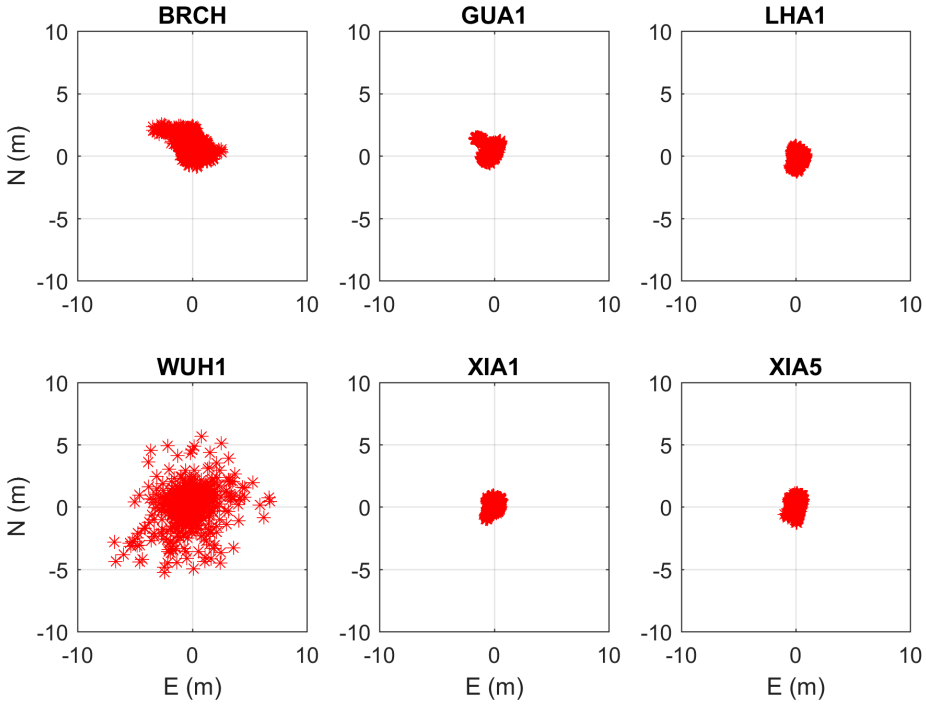

Figure 28. Horizontal positioning error scatter plots of B1I SPP with TGD correction for the six selected stations. In each plot, the horizontal and vertical axes indicate the E component error and the N component error, respectively (unit: m).

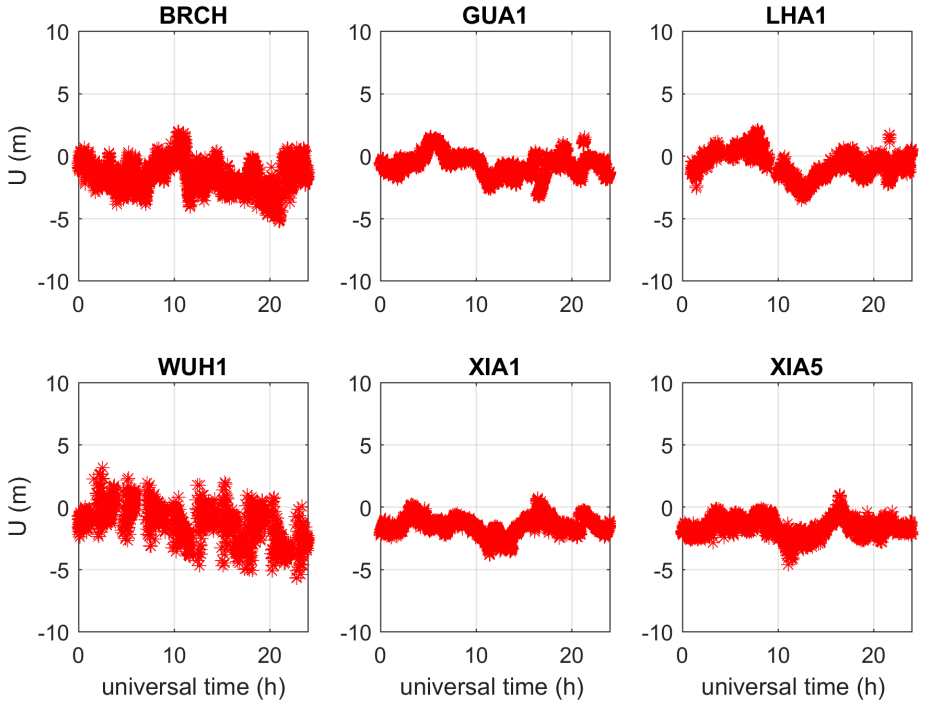

Figure 29. Vertical positioning error scatter plots of B1I SPP with TGD correction for the six selected stations. In each plot, the horizontal and vertical axes indicate the universal time (h) and the U component error, respectively (unit: m).

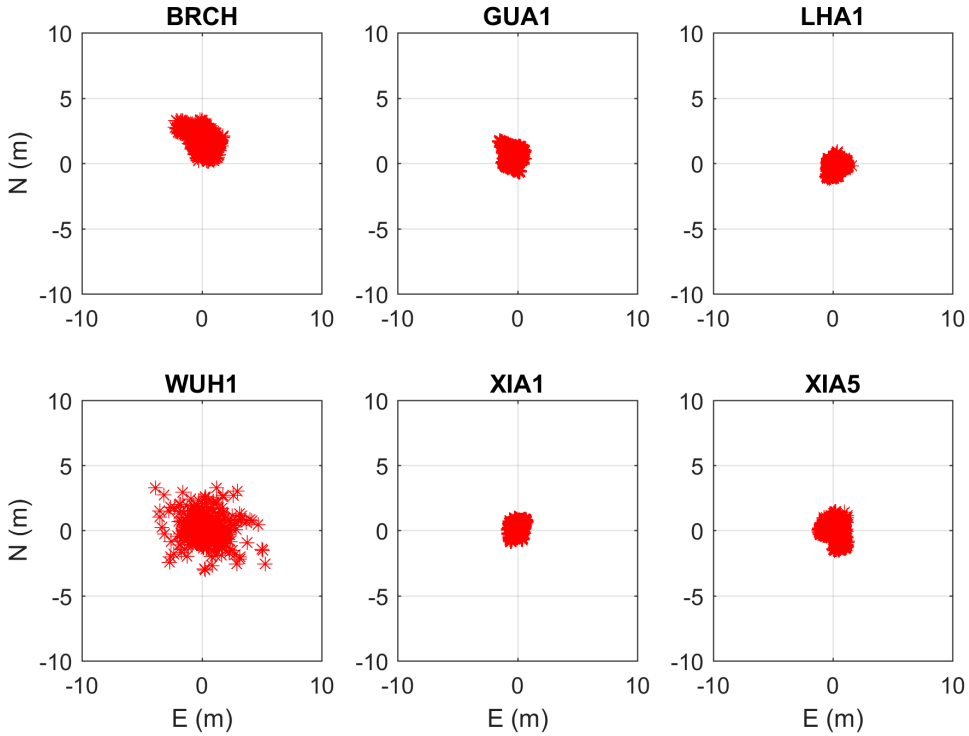

Figure 30. Horizontal positioning error scatter plots of B3I SPP with TGD correction for the six selected stations. In each plot, the horizontal and vertical axes indicate the E component error and the N component error, respectively (unit: m).

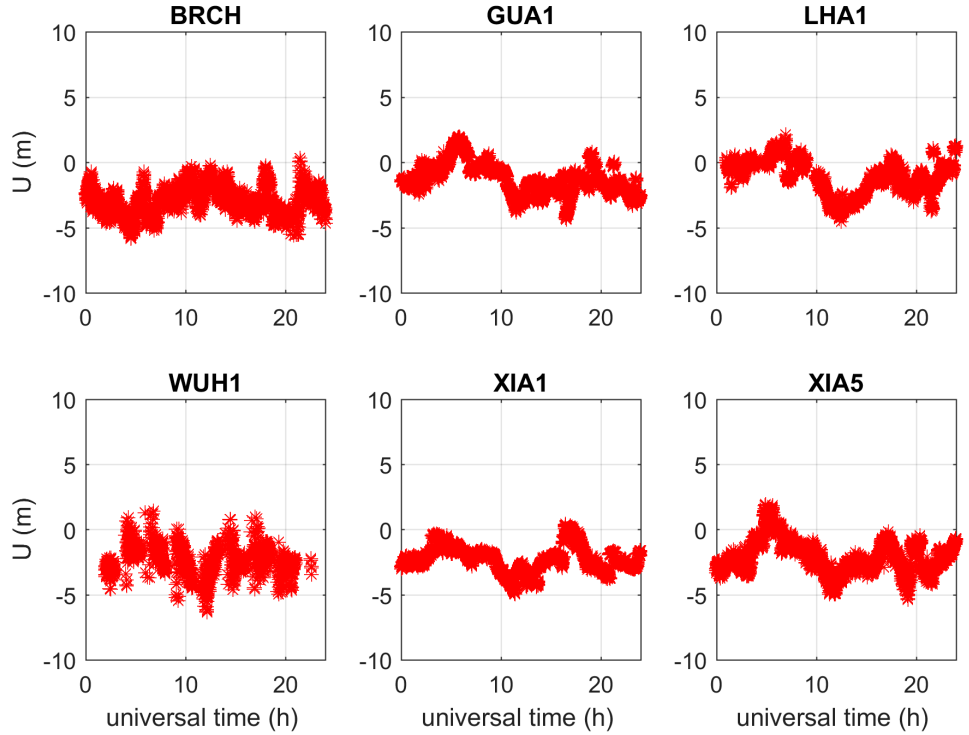

Figure 31. Vertical positioning error scatter plots of B3I SPP with TGD correction for the six selected stations. In each plot, the horizontal and vertical axes indicate the universal time (h) and the U component error, respectively (unit: m).

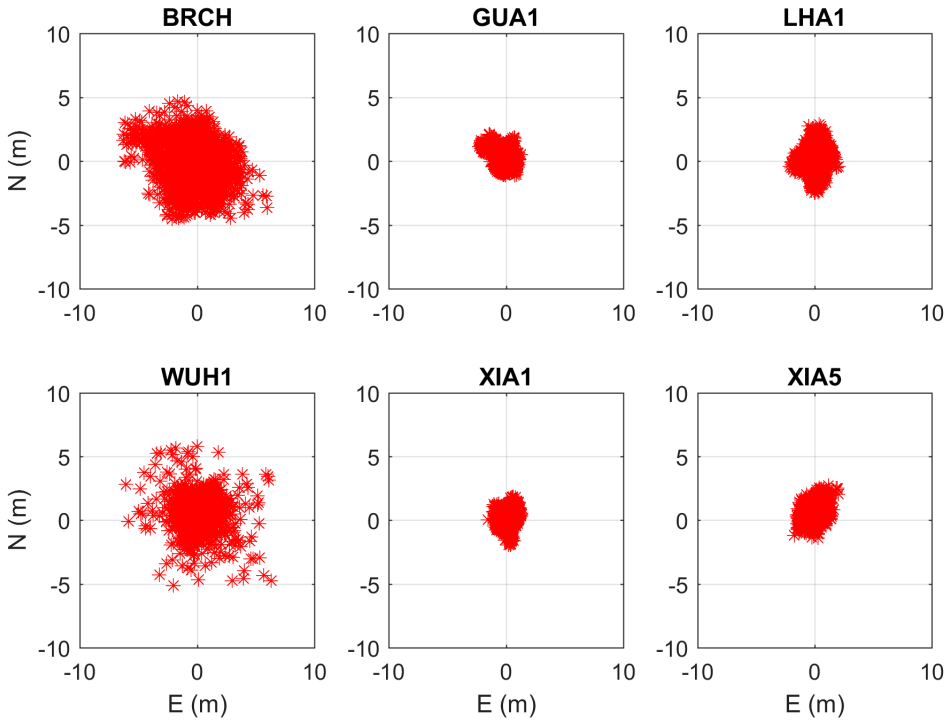

Figure 32. Horizontal positioning error scatter plots of B1I/B3I SPP with TGD correction for the six selected stations. In each plot, the horizontal and vertical axes indicate the E component error and the N component error, respectively (unit: m).

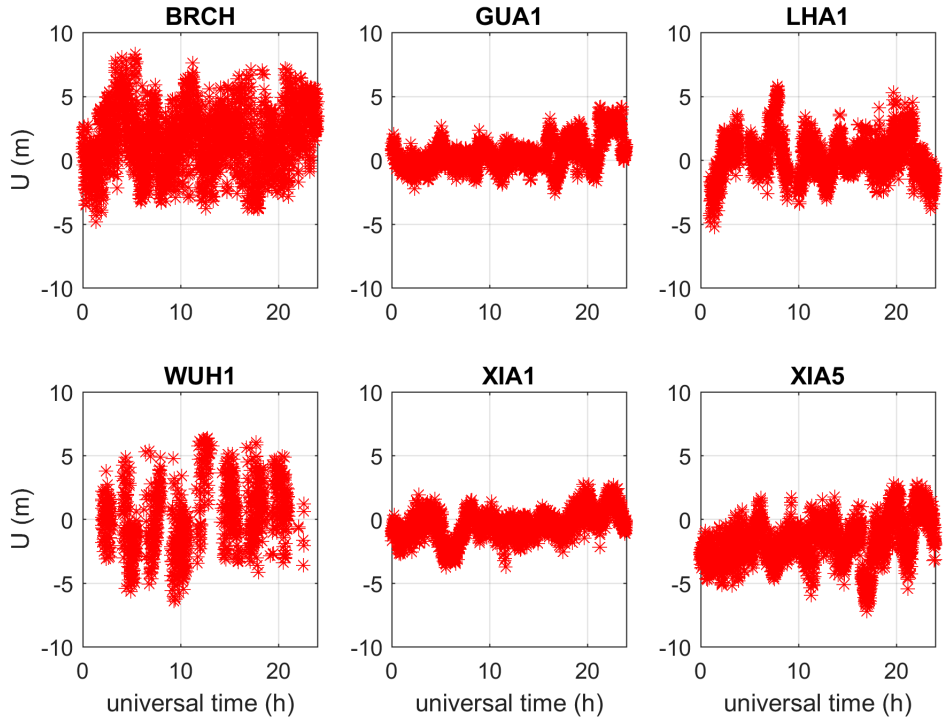

Figure 33. Vertical positioning error scatter plots of B1I/B3I SPP with TGD correction for the six selected stations. In each plot, the horizontal and vertical axes indicate the universal time (h) and the U component error, respectively (unit: m).

To further evaluate the impact of the TGD parameters on the positioning accuracy of BDS-2 + BDS-3, the daily RMS values for each station are calculated (Figure 34), and the mean values for all

stations are shown in Table 7. Compared with BDS-2 and BDS-3, we can conclude that the positioning accuracy of the BDS-2 + BDS-3 combination system performs better than BDS-2 or BDS-3. Moreover, the single- and dual-frequency positioning errors of BDS-2+BDS-3 can reach 1 m–2 m. We expect that BDS-2 + BDS-3 can achieve a better performance when the global system will be completed in 2020.

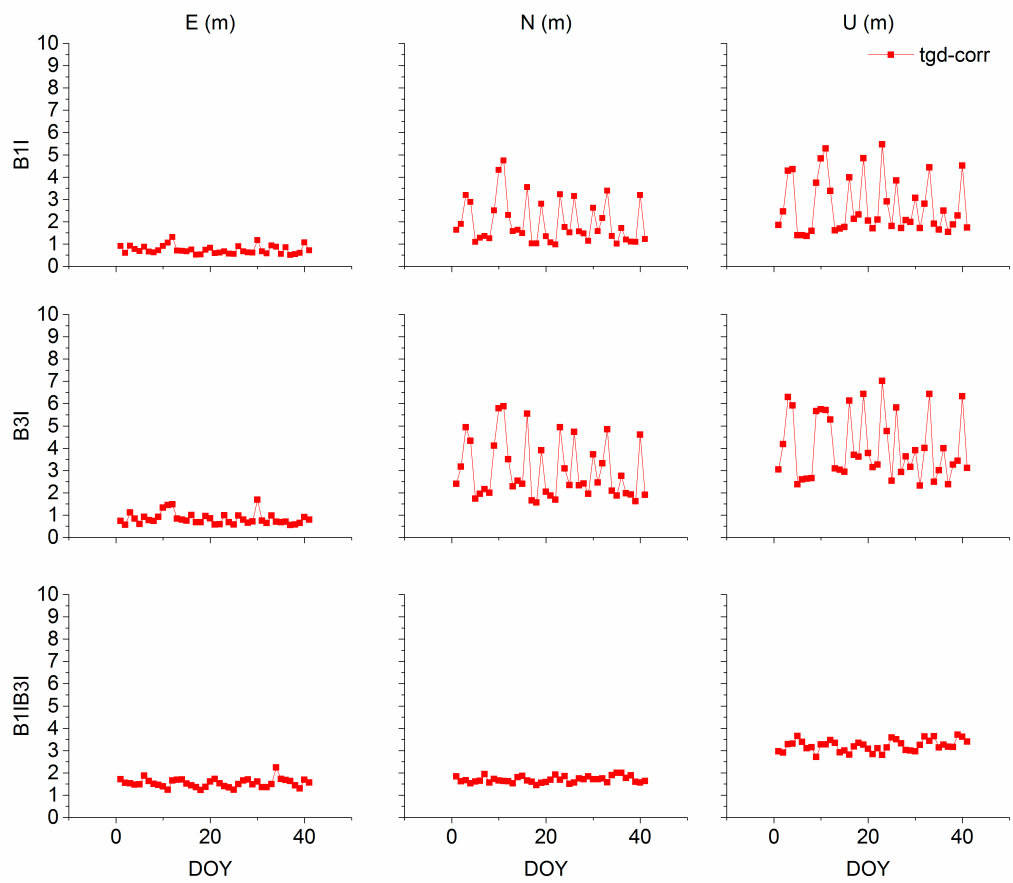

Figure 34. Daily RMSs of BDS-2 + BDS-3 at the BRCH station with TGD correction.

Table 7. The mean RMS values of all the SPP solutions with TGD correction (m).

Scheme		B1I	B3I	B1I/B3I
E	tgd-corr	0.86	-	1.18
	non-corr	-	0.90	-
N	tgd-corr	0.85	-	1.08
	non-corr	-	1.07	-
U	tgd-corr	1.84	-	2.17
	non-corr	-	2.56	-

5. Conclusions

China's BDS-3 system is rapidly developing; from November 2017 to May 2019, 18 MEO, 1 GEO and 1 IGSO BDS-3 satellites (excluding experimental satellites) have been successfully launched. As a global system, BDS-3 has already provided basic services to the countries along the Belt and Road and to the neighbouring regions since the end of 2018. This work aims to investigate the impact of TGD on BDS-2, BDS-3 and BDS-2 + BDS-3 positioning. In this contribution, the single- and dual-frequency positioning accuracy of the BDS-3 signals were analysed. Six iGMAS stations, which can receive all the BDS-2 and BDS-3 signals at the current stage, with 41-day observation data, were selected to support our findings.

Single- (B1I, B3I, B1C and B2a) and dual-frequency (B1I/B3I and B1C/B2a) BDS-2, BDS-3 and BDS-2 + BDS-3 combined system signals were assessed with and without TGD correction. The results showed that the RMS value of B1I SPP with the "tgd-corr" scheme was increased by approximately 50% compared with the "non-corr" scheme based on BDS-2 satellites. For the positioning accuracy of all BDS-3 signals, the single- and dual-frequency-based SPP solutions without TGD correction present systematic errors deviating from the true positions. The accuracy of B1I SPP is improved by approximately 68.0%, 69.2% and 49.2% with TGD correction in the N, E and U components respectively, compared to SPP without TGD correction. The positioning accuracy of B1C SPP with the "tgd-corr" scheme is reduced by 64.8% from 1.18 m to 3.35 m and by 64.4% from 1.48 m to 4.16 m and by 51.2% from 2.91 m to 5.96 m in the E, N and U components, respectively. The RMS of B2a SPP is significantly reduced by 60.2% from 2.84 m to 1.13 m, by 55.4% from 3.59 m to 1.60 m and by 19.8% from 5.09 m to 4.18 m in E, N and U components, respectively. Compared with the "non-corr" scheme, the RMS of B1I/B3I SPP is reduced by 75%, 71.0% and 45.4% in the horizontal and vertical components, and the positioning accuracy can reach 1 m–2 m after TGD correction. The positioning accuracy of B1C/B2a SPP with the "tgd-corr" scheme is improved by 66.1% and 62.1% in the horizontal components. The N and E components can reach 1.66 m and 1.85 m, respectively, and the vertical component is improved by 43.3%, from 6.31 m to 3.58 m. The regional limitations of BDS-2 were overcome when BDS-3 satellites were put into use; hence, the global positioning accuracy of the BDS-2 + BDS-3 combined system is better than that of the BDS-2 or BDS-3. We expect that a better performance of BDS-3 can be reached when the global system completed.

Author Contributions: P.D., Y.G., W.Q. and X.Y. conceived and designed the experiments; P.D. performed the experiments, analyzed the data, and wrote the paper; X.Y. and Y.G. helped in the discussion and revision.

Funding: This work was supported by the National Natural Science Foundation of China (No. 11703033), Natural Science Foundation of Shaanxi (No.2018JQ1020) and Youth promotion committee of Chinese Academy of Sciences. The authors acknowledge iGMAS for funding.

Acknowledgments: The authors gratefully acknowledge iGMAS and IGS for providing broadcast ephemeris, data, and satellite information.

Conflicts of Interest: The authors declare no conflict of interest.

References

1. Lou, Y.; Liu, Y.; Shi, C.; Yao, X.; Zheng, F. Precise orbit determination of BeiDou constellation based on BETS and MGEX network. *Sci. Rep.* **2014**, *4*, 4692. [CrossRef] [PubMed]
2. Yang, Y.; Xu, Y.; Li, J.; Yang, C. Progress and performance evaluation of BeiDou global navigation satellite system: Data analysis based on BDS-3 demonstration system. *Sci. China Earth Sci.* **2018**, *6*, 614–624. [CrossRef]
3. Li, X.; Yuan, Y.; Zhu, Y.; Huang, J.; Wu, J.; Xiong, Y.; Zhang, X.; Li, X. Precise orbit determination for BDS3 experimental satellites using iGMAS and MGEX tracking networks. *J. Geod.* **2018**, *93*, 103–117. [CrossRef]
4. Ge, Y.; Yang, X.; Qin, W.; Su, H.; Wu, M.; Wang, Y.; Wang, S. Time Transfer Analysis of GPS- and BDS-Precise Point Positioning Based on iGMAS Products. *China Satell. Navig. Conf.* **2018**, *497*, 519–530.
5. Ge, Y.; Yang, X.; Qin, W.; Yang, H.; Guang, W.; Zhou, F.; Ouyang, M.; Wang, S. Mitigation of the multipath effect in BDS-based time transfer using a wave-absorbing shield. *Adv. Space Res.* **2018**, *63*, 2771–2783. [CrossRef]
6. Chu, F.Y.; Yang, M. BeiDou System (BDS) Triple-Frequency Ambiguity Resolution without Code Measurements. *Remote Sens.* **2018**, *10*, 675. [CrossRef]
7. Zhao, Q.; Guo, J.; Li, M.; Qu, L.; Hu, Z.; Shi, C.; Liu, J. Initial results of precise orbit and clock determination for COMPASS navigation satellite system. *J. Geod.* **2013**, *87*, 475–486. [CrossRef]
8. Li, X.; Zhang, X.; Ren, X.; Fritsche, M.; Wickert, J.; Schuh, H. Precise positioning with current multi-constellation Global Navigation Satellite Systems: GPS, GLONASS, Galileo and BeiDou. *Sci. Rep.* **2015**, *5*, 8328. [CrossRef]
9. Guo, F.; Li, X.; Zhang, X.; Wang, J. The contribution of Multi-GNSS Experiment (MGEX) to precise point positioning. *Adv. Space Res.* **2016**, *59*, 2714–2725. [CrossRef]
10. Guo, F.; Zhang, X.; Wang, J. Timing group delay and differential code bias corrections for BeiDou positioning. *J. Geod.* **2015**, *89*, 427–445. [CrossRef]

11. Zhang, X.; He, X. Performance analysis of triple-frequency ambiguity resolution with BeiDou observations. *GPS Solut.* **2015**, *20*, 269–281. [CrossRef]
12. Manzino, A.M.; Dabove, P.; Gogoi, N. Assessment of positioning performances in Italy from GPS, BDS and GLONASS constellations. *Geod. Geodyn.* **2018**, *9*, 439–448. [CrossRef]
13. Wanninger, L.; Beer, S. BeiDou satellite-induced code pseudorange variations: diagnosis and therapy. *GPS Solut.* **2015**, *19*, 639–648. [CrossRef]
14. Mao, Y.; Wang, Q.; Hu, C.; He, Y. Accuracy Analysis of BDS-3 Experiment Satellite Broadcast Ephemeris. *China Satell. Navig. Conf.* **2018**, *498*, 341–354.
15. Wu, Z.; Zhou, S.; Hu, X.; Liu, L.; Shuai, T.; Xie, Y.; Tang, C.; Pan, J.; Zhu, L.; Chang, Z. Performance of the BDS3 experimental satellite passive hydrogen maser. *GPS Solut.* **2018**, *22*. [CrossRef]
16. Xu, X.; Li, M.; Li, W.; Liu, J. Performance Analysis of Beidou-2/Beidou-3e Combined Solution with Emphasis on Precise Orbit Determination and Precise Point Positioning. *Sensors (Basel)* **2018**, *18*, 135. [CrossRef] [PubMed]
17. Zhao, Q.; Wang, C.; Guo, J.; Wang, B.; Liu, J. Precise orbit and clock determination for BeiDou-3 experimental satellites with yaw attitude analysis. *GPS Solut.* **2017**, *22*. [CrossRef]
18. Zhou, R.; Hu, Z.; Zhao, Q.; Li, P.; Wang, W.; He, C.; Cai, C.; Pan, Z. Elevation-dependent pseudorange variation characteristics analysis for the new-generation BeiDou satellite navigation system. *GPS Solut.* **2018**, *22*. [CrossRef]
19. Li, X.; Xie, W.; Huang, J.; Ma, T.; Zhang, X.; Yuan, Y. Estimation and analysis of differential code biases for BDS3/BDS2 using iGMAS and MGEX observations. *J. Geod.* **2018**, *93*, 419–435. [CrossRef]
20. CSNO. *BeiDou Navigation Satellite System Signal in Space Interface Control Document, Open Service Signal B3I (Version 1.0)*; China Satellite Navigation Office: Beijing, China, February 2018.
21. CSNO. *BeiDou Navigation Satellite System Signal in Space Interface Control Document, Open Service Signal B1C (Version 1.0)*; China Satellite Navigation Office: Beijing, China, December 2017.
22. CSNO. *BeiDou Navigation Satellite System Signal in Space Interface Control Document, Open Service Signal B2a (Version 1.0)*; China Satellite Navigation Office: Beijing, China, December 2017.
23. Xie, X.; Fang, R.; Geng, T.; Wang, G.; Zhao, Q.; Liu, J. Characterization of GNSS Signals Tracked by the iGMAS Network Considering Recent BDS-3 Satellites. *Remote Sens.* **2018**, *10*, 1736. [CrossRef]
24. Ye, F.; Yuan, Y.; Ou, J. Initial orbit determination of BDS-3 satellites based on new code signals. *Geod. Geodyn.* **2018**, *9*, 342–346. [CrossRef]
25. Leick, A.; Rapoport, L.; Tatarnikov, D. *GPS Satellite Surveying, Fourth Edition*; Wiley: Hoboken, NJ, USA, 2015.
26. Ge, Y.; Zhou, F.; Sun, B.; Wang, S.; Shi, B. The Impact of Satellite Time Group Delay and Inter-Frequency Differential Code Bias Corrections on Multi-GNSS Combined Positioning. *Sensors (Basel)* **2017**, *17*, 602. [CrossRef] [PubMed]
27. CSNO. *BeiDou Navigation Satellite System Signal in Space Interface Control Document-Open Service Signal, Version 2.0*; China Satellite Navigation Office: Beijing, China, December 2013.
28. Hernández-Pajares, M.; Juan, J.M.; Sanz, J.; Orus, R.; Garcia-Rigo, A.; Feltens, J.; Komjathy, A.; Schaer, S.C.; Krankowski, A. The IGS VTEC maps: A reliable source of ionospheric information since 1998. *J. Geod.* **2009**, *83*, 263–275. [CrossRef]
29. CSNO. *BeiDou Navigation Satellite System Signal in Space Interface Control Document-Open Service Signal B1I, Version 1.0*; China Satellite Navigation Office: Beijing, China, December 2012.
30. CSNO. *BeiDou Navigation Satellite System Open Service Performance Standard, Version 2.0*; China Satellite Navigation Office: Beijing, China, December 2018.
31. Jiao, G.; Song, S.; Ge, Y.; Su, K.; Liu, Y. Assessment of BeiDou-3 and Multi-GNSS Precise Point Positioning Performance. *Sensors* **2019**, *19*, 2496. [CrossRef] [PubMed]
32. Ferland, R.; Piraszewski, M. The IGS-combined station coordinates, earth rotation parameters and apparent geocenter. *J. Geod.* **2009**, *83*, 385–392. [CrossRef]
33. Cai, H.; Chen, K.; Xu, T.; Chen, G. The iGMAS Combined Products and the Analysis of Their Consistency. In Proceedings of the China Satellite Navigation Conference (CSNC), Xi'an, China, 13–15 May 2015.